

1 **Title page**

2 **Viral RNA switch mediates the dynamic control of flavivirus**

3 **replicase recruitment by genome cyclization**

4 Zhong-Yu Liu,^{1,2} Xiao-Feng Li,^{1,2} Tao Jiang,^{1,2} Yong-Qiang Deng,^{1,2} Qing Ye,¹ Hui Zhao,¹

5 Jiu-Yang Yu,¹ and Cheng-Feng Qin^{1,2*}

6 ¹Department of Virology, Beijing Institute of Microbiology and Epidemiology, Beijing

7 100071, China; ²State Key Laboratory of Pathogen and Biosecurity, Beijing 100071 China;

8 *Corresponding author. C.F. Qin: Department of Virology, Beijing Institute of Microbiology

9 and Epidemiology, Beijing 100071, China. Email: gincf@bmi.ac.cn

10 Number of Figures: 12

11 Word counts: 5625

12 Running title: Dynamic replicase recruitment by flavivirus RNA switch.

13 **Abstract**

14 Viral replicase recruitment and long-range RNA interactions are essential for RNA virus
15 replication, yet the mechanism of their interplay remains elusive. Flaviviruses include
16 numerous important human pathogens, e.g., dengue virus (DENV) and Zika virus (ZIKV).
17 Here, we revealed a highly conserved, conformation-tunable *cis*-acting element named
18 5'-UAR-flanking stem (UFS) in the flavivirus genomic 5' terminus. We demonstrated that
19 the UFS was critical for efficient NS5 recruitment and viral RNA synthesis in different
20 flaviviruses. Interestingly, stabilization of the DENV UFS impaired both genome cyclization
21 and vRNA replication. Moreover, the UFS unwound in response to genome cyclization,
22 leading to the decreased affinity of NS5 for the viral 5' end. Thus, we propose that the UFS
23 is switched by genome cyclization to regulate dynamic RdRp binding for vRNA replication.
24 This study demonstrates that the UFS enables communication between flavivirus genome
25 cyclization and RdRp recruitment, highlighting the presence of switch-like mechanisms
26 among RNA viruses.

27 **Introduction**

28 *Cis*-acting regulatory elements play essential yet diverse roles in the life cycle of RNA
29 viruses (*Liu et al., 2009; Nicholson and White, 2014*). These elements have been found to
30 regulate viral replicase binding and viral RNA (vRNA) synthesis (*Filomatori et al., 2006;*
31 *Vogt and Andino, 2010; Wu et al., 2009*), nucleocapsid assembly (*Goto et al., 2013;*
32 *Keane et al., 2015; Morales et al., 2013*), and viral translation (*Brierley and Dos Ramos,*
33 *2006; Kieft, 2008; Liu et al., 2009; Simon and Miller, 2013*). In particular, local RNA
34 elements in viral genomes are often involved in long-range RNA-RNA interactions
35 (*Alvarez et al., 2005; Nicholson and White, 2014; Shetty et al., 2013*), which are often
36 referred to as genome cyclization and can bring regions separated by several thousand
37 nucleotides into proximity. Such strategies have been observed in different classes of
38 RNA viruses and play different roles in virus propagation (*Nicholson and White, 2014*). In
39 fact, the entire genomes of some RNA viruses are highly structured and have complex
40 global architecture (*Athavale et al., 2013; Wu et al., 2013*).

41 The genus flavivirus includes important causative agents for human diseases, such as
42 dengue virus (DENV1-4), West Nile virus (WNV), Japanese encephalitis virus (JEV),
43 yellow fever virus (YFV) and the emerging Zika virus (ZIKV) (*Fauci and Morens, 2016;*
44 *Mlakar et al., 2016*). Major phylogenetic groups (*Blitvich and Firth, 2015; Moureau et al.,*
45 *2015*) of flaviviruses include mosquito-borne flaviviruses (MBFVs), tick-borne flaviviruses
46 (TBFVs), insect-specific flaviviruses (ISFVs) and flaviviruses with no known vectors
47 (NKVs). Leading to diseases with symptoms ranging from mild fever and rash to severe
48 hemorrhagic fever and encephalitis, the emergence and re-emergence of flaviviruses

49 always arouses global concern. The flaviviruses are single-stranded, positive-sense RNA
50 viruses, and their genome is approximately 11 kb and contains a single ORF, which
51 encodes a polyprotein precursor with more than 3,000 residues. The precursor is further
52 processed into 3 structural proteins (capsid, pre-membrane/membrane and envelope) and
53 at least 7 nonstructural proteins (NS1, NS2A, NS2B, NS3, NS4A, NS4B and NS5). The
54 largest nonstructural protein, NS5, performs methyltransferase (*Egloff et al., 2002; Zhou*
55 *et al., 2007*), guanylyltransferase (*Issur et al., 2009*) and RNA-dependent RNA
56 polymerase (RdRp) activity (*Nomaguchi et al., 2003; Uchil and Satchidanandam, 2003;*
57 *Yap et al., 2007*). NS5 interacts with vRNA, other viral nonstructural proteins and host
58 factors to assemble to the viral replication complex essential for vRNA synthesis (*Klema et*
59 *al., 2015*). On the other hand, the highly structured 5' and 3' untranslated regions (UTRs)
60 occupy the termini of the viral genome (*Friebe and Harris, 2010; Gebhard et al., 2011;*
61 *Villordo et al., 2016*) and contain *cis*-acting elements crucial for vRNA replication (*Clyde et*
62 *al., 2008; Filomatori et al., 2006; Liu et al., 2013; Lodeiro et al., 2009; Rouha et al., 2011;*
63 *Villordo et al., 2010*), translation (*Chiu et al., 2005; Clyde and Harris, 2006*), viral
64 pathogenesis (*Chapman et al., 2014; Funk et al., 2010; Roby et al., 2014*) and host
65 adaptation (*Villordo et al., 2015*).

66 Hybridization of complementary sequences at the 5' and 3' termini, which include the
67 5'-3' upstream AUG region (UAR) (*Alvarez et al., 2005; Zhang et al., 2008*), downstream
68 AUG region (DAR) (*Friebe and Harris, 2010; Friebe et al., 2011*) and cyclization sequence
69 (CS) (*Khromykh et al., 2001*) elements, circularizes the genome of MBFV. Genome
70 cyclization, which is also modulated by the downstream of 5' CS pseudoknot (DCS-PK) in

71 the capsid-coding region (*de Borba et al., 2015; Liu et al., 2013*), is crucial for the
72 translocation of NS5 from the 5' stem-loop A (SLA) promoter to the RNA synthesis
73 initiation site at the 3' end (*Filomatori et al., 2006*). However, the mechanistic details of this
74 critical process are poorly understood. The 5' SLA structure and genome cyclization
75 strategy were also identified in other phylogenetic groups of the flavivirus genus, although
76 the specific details differ. The 5' UAR element in MBFV usually participates in the
77 formation of a local hairpin, stem-loop B (SLB), in the linear conformation of the vRNA.
78 The SLA and SLB elements are separated by a short uracil-rich sequence, which has
79 been shown to mediate vRNA replication of DENV (*Lodeiro et al., 2009*). In the present
80 study, we demonstrated that the U-rich region of MBFV is involved in the formation of a
81 conserved RNA duplex that is designated as a 5'-UAR-flanking stem (UFS) because it
82 locks the 5' UAR/SLB element between its two strands. A combination of our results
83 suggested that the UFS and its cousin elements regulate the binding of viral RdRp to
84 vRNA dynamically by switching their conformations in response to the long-range
85 interactions between the viral 5' and 3' ends. Furthermore, UFS switching is a general
86 replication strategy in flaviviruses with vertebrate hosts, highlighting their role in the host
87 adaptation and evolution of flaviviruses.

88 **Results**

89 **The UFS structure is conserved among the flavivirus genus**

90 Although the U-rich region in the 5' end of the MBFV genome has been shown to
91 enhance vRNA replication (*Friebe and Harris, 2010; Lodeiro et al., 2009*), there were
92 controversial opinions regarding the detailed structures downstream of SLA in flaviviruses

93 (Dong et al., 2008; Gebhard et al., 2011; Liu et al., 2013; Villordo and Gamarnik, 2009;
94 Zhang et al., 2008). To clarify the structural characteristics of the region downstream of
95 SLA, representative sequences derived from various flavivirus species were subjected to
96 the *mfold* RNA folding server (Zuker, 2003; Zuker and Jacobson, 1998). Because the
97 region of interest is involved in genome cyclization, both the 5' end sequences and the
98 query sequences composed of the 5' end and 3' UTR were analyzed. *Figure 1A* shows the
99 representative results of the RNA structure prediction. The local RNA structures in the 5'
100 and 3' ends of DENV4 vRNA are demonstrated, and elements involved in long-range
101 interactions are highlighted. Structure prediction of the 5' end local structures showed that
102 the U-rich region of most MBFVs (except the YFV clade) forms a duplex with
103 complementary sequences in or near the viral translational starting region (*Figure 1B*).
104 Because this duplex confines the 5' UAR/SLB element between its two strands, we
105 designated it as the UFS. Furthermore, the UFS duplex was predicted to unwind due to
106 the formation of the panhandle structure between the 5' and 3' ends when long-range
107 interactions between the genome termini were considered (*Figure 1 - figure supplement 1*
108 *and Supplementary file 1*).

109 Because the local folding pattern of the 5' end and the mode of genome cyclization in
110 the YFV clade are different than those in other MBFVs (*Figure 1B*), the corresponding
111 hairpin including the U-rich region in the YFV clade was recognized as ψ UFS. Local
112 structures similar to UFS were also identified in ISFVs (*Figure 1B*) and Modoc virus
113 (MODV) among the NKVs (*Figure 1B*), whereas the non-vectored Rio Bravo virus (RBV,
114 *Figure 1B*) was shown to contain a ψ UFS structure. The UFS and ψ UFS in NKVs were

115 also involved in genome cyclization, similar to the corresponding structures in MBFVs. In
116 contrast, the UFS-like structures were not predicted to be involved in genome cyclization
117 in ISFVs, suggesting that the UFS in MBFVs and UFS-like structures in ISFVs function
118 differently. Finally, the UFS/ ψ UFS structure was not identified in TBFVs or in the Yokose
119 virus clade of NKVs; instead, a short hairpin with a large loop occupied the analogous
120 location of the UFS in these viruses (*Supplementary file 2*). Taken together, the above
121 results demonstrated the conservation of UFS elements among the flavivirus genus and
122 suggested that the secondary structures of UFS elements are affected by genome
123 conformation.

124 ***In vitro* formation of UFS duplexes in different flaviviruses**

125 To investigate whether the duplex conformation of the UFS can indeed exist locally
126 under *in vitro* conditions, RNA molecules corresponding to the 5' ends of DENV1-4, JEV
127 and ZIKV were analyzed by selective 2'-hydroxyl acylation analyzed by primer extension
128 (SHAPE). The SHAPE reactivity data were annotated on RNA structure models generated
129 by *mfold* prediction and sequence comparison (*Figure 2*). The SHAPE results were shown
130 to agree well with the predicted RNA structures. It was shown that the UFS element of
131 JEV forms a conical duplex structure under *in vitro* conditions (*Figure 2A*) because all
132 nucleotides of the UFS exhibited low SHAPE reactivity. Similar results were obtained for
133 ZIKV and DENV serotypes 1, 3 and 4 (*Figure 2B, 2D, 2E and 2F*), except that several
134 nucleotides in the ZIKV and DENV1/3 UFS regions had elevated SHAPE reactivity, which
135 was likely due to the presence of internal loops. In contrast, the SHAPE results indicated
136 that the UFS duplex of DENV2 is highly unstable because the DENV2 UFS region showed

137 considerable SHAPE reactivity (*Figure 2C*). This result was consistent with
138 thermodynamic calculations and suggested that the UFS duplex is a highly dynamic
139 structure, at least in some flaviviruses. The presence of the DENV UFS duplex
140 conformation was further confirmed by SHAPE analysis of DENV3 5' end RNA molecules
141 containing mutations in the UFS (*Figure 2 - figure supplement 1*). It was shown that the
142 SHAPE reactivity of the UFS region significantly increased in UFS-disrupted mutants
143 (*Figure 2 - figure supplement 1, D3-M13A and D3-M13B*), and restoration of UFS
144 base-pairing endowed the corresponding region with low SHAPE reactivity (*Figure 2 -*
145 *figure supplement 1, D3-M13C*). The above results demonstrated that the UFS duplex can
146 exist locally in the vRNA 5' end under *in vitro* conditions, suggesting that the UFS can
147 assume the duplex conformation, at least under certain states of the flavivirus genome.

148 **The UFS duplex is critical for efficient vRNA replication**

149 The UFS is located just downstream of the SLA promoter element, and it interlocks
150 with cyclization sequences in the vRNA 5' end. This peculiar localization of the UFS
151 suggests a unique role in vRNA replication. Functional mutagenesis of the UFS was
152 performed using a DENV4 replicon with internal ribosome entry site (IRES)-controlled viral
153 translation (*Liu et al., 2013*). To eliminate the possibility that productive 5'-cap-directed
154 translation is caused by mutations altering the start codon (*Clyde and Harris, 2006*), which
155 is embedded in the DENV4 UFS duplex, a nonsense mutation was introduced into the
156 variable loop 3 of DCS-PK in the background of p4-chPstop-SP-IRES-Rluc-Rep to
157 generate the p4-Dualstop-SP-IRES-Rluc-Rep replicon (*Figure 3A*). The replication
158 characteristics of the two replicons were basically the same (*Figure 3B*). First, a panel of

159 mutants was generated, and their replication efficiency was assessed in BHK-21 cells.
160 Disrupting the base-pairing of the UFS (*Figure 3C, D. M1A, M1B, M3A and M3B*) greatly
161 reduced vRNA replication, whereas reconstituting base-pairing by combining the
162 corresponding mutations was able to restore vRNA replication (*Figure 3C, D. M1C and*
163 *M3C*), although the M3C mutant replicated moderately less efficiently than the wild-type
164 (WT) replicon, possibly due to the apparent primary sequence changes in the U-rich
165 region. Next, the impact of the M1 and M3 mutations on the circularized vRNA structure
166 was assessed using the *mfold* online server. It was shown that the overall genome
167 cyclization pattern was only slightly affected by the M1 and M3 mutations (*Supplementary*
168 *file 3*), and the changes in the stability of the predicted circularized structures was
169 considerable smaller than the changes in the local UFS structure. To further confirm the
170 function of local UFS structure in vRNA replication, we designed a panel of mutations
171 (*Figure 3 - figure supplement 1*), which neither affected vRNA cyclization pattern nor the
172 internal loop structure in the circular form, and the corresponding mutants were assessed
173 for replication efficiency. It was shown that disruption of UFS base pairing (*mutant AGU*
174 *and GAU*) reduced vRNA replication greatly, whereas substituting of a few base pairs in
175 the UFS (*mutant AUA and ACG*) only have moderate effects on vRNA replication.

176 To confirm that the RNA conformation was changed as expected by the corresponding
177 mutations, SHAPE analysis was performed for DENV4 5'-300 nt RNA containing the M1A,
178 M1C, M3A or M3C mutation, and the SHAPE results were compared with WT RNA (*Figure*
179 *4*). In WT RNA, nucleotides composing the UFS only showed low or background SHAPE
180 reactivity, whereas the SHAPE reactivity of the UFS region increased significantly in the

181 M1A and M3A mutants, suggesting that the UFS duplex was indeed disrupted by the
182 corresponding mutations. In contrast, the M1C and M3C mutations greatly reduced the
183 SHAPE reactivity of the UFS region. RNA structure predictions using the *RNAstructure*
184 (*Reuter and Mathews, 2010*) software with SHAPE constraints confirmed that the UFS
185 structure was disrupted/destabilized or reconstituted as aimed, and these mutations did
186 not affect the overall secondary structure of the 5' end RNA (*Supplementary file 4*). Taken
187 together, the above results demonstrated that the presence of the UFS greatly enhances
188 vRNA replication, and this function is directly correlated to its duplex conformation.

189 **The function of the UFS is crucial for viral propagation of flavivirus**

190 We further attempted to investigate the influence of the UFS on the propagation of
191 infectious virus. Various mutations targeting the UFS element (*Figure 3 and 5A*) were
192 introduced into a DENV4 infectious clone. vRNA copies in BHK-21 cells were determined
193 at different time points post-electroporation (*Figure 5B-D*). It was shown that the vRNA
194 copies in BHK-21 cells transfected with the M1A, M3A or M5A mutants were significantly
195 lower than those transfected with WT vRNA at 48-72 h post-transfection, whereas
196 restoration of the UFS element by complementary mutations partially (*Figure 5C, M3C*) or
197 fully (*Figure 5B, D. M1C and M5C*) recovered the vRNA replication levels, highlighting the
198 importance of the UFS for vRNA replication of infection-competent viruses. An indirect
199 immunofluorescence assay (IFA, *Figure 5E*) revealed that the DENV-positive rates were
200 apparently lower in cells transfected with UFS-disrupted mutants than in those transfected
201 with UFS-restored mutants or WT vRNA at the same time points. The virus titers in the
202 culture supernatants of M1A-transfected BHK-21 cells were also significantly lower than

203 those of M1C- or WT-transfected cells (*Figure 5F*).

204 The effect of UFS mutations on vRNA stability was then assessed. To this end, DENV4
205 NS5-GVD-vRNAs containing different UFS mutations were transfected into BHK-21 cells
206 by electroporation, and vRNA copies were determined at 4, 24, 48 and 72 h
207 post-transfection. Only negligible differences in RNA stability were found between WT
208 RNA and the mutants of the M1 or M3 groups (*Figure 5G,H*), and the stability of the M5C
209 mutant was moderately reduced compared with that of the M5A mutant (*Figure 5I*). Thus,
210 the differences in the RNA stability of the UFS mutants did not account for their different
211 replication characteristics. The above results demonstrated that the UFS element is
212 required for virus propagation due to its function in vRNA replication. In agreement with
213 the function of DENV4 UFS, we also showed that disrupting of the UFS greatly reduced
214 viral propagation of ZIKV, whereas reconstitution of the UFS duplex restores ZIKV
215 propagation by IFA tests performed in transfected BHK-21 cells (*Figure 5 - figure*
216 *supplement 1*).

217 **The duplex conformation of the UFS is required for robust NS5Pol binding and** 218 **RdRp activity**

219 To understand the mechanism of how the UFS fulfills its role in vRNA replication, a
220 series of *in vitro* assays were performed (*Figure 6*). Because NS5 encodes the RdRp
221 activity required for vRNA synthesis and has specific interactions with the 5' end of vRNA
222 (*Dong et al., 2008; Filomatori et al., 2006; Lodeiro et al., 2009*), whether the UFS is
223 involved in the recruitment of NS5 was examined. WT and UFS-mutated DENV4 5'-300 nt
224 RNA molecules were incubated with different concentrations of the NS5 RdRp domain

225 (NS5Pol), and the reaction mixtures were analyzed by native PAGE. The binding of
226 NS5Pol to 5'-300 nt RNA containing the M1A or M1B mutation in UFS was much weaker
227 than the binding to 5'-300 nt WT RNA, whereas the 5'-300 nt M1C and WT RNA bound to
228 NS5Pol with comparable affinity (*Figure 6C, top and middle panels*). The 5'-300 nt M3A
229 and M3B RNA also interacted with NS5Pol weakly, whereas the combination of the two
230 mutations apparently restored the interaction between NS5Pol and 5'-300 nt M3C RNA
231 (*Figure 6C, bottom panel*). The above results indicated that the UFS duplex is required for
232 efficient NS5Pol binding. Moreover, EMSA assay demonstrated that the UFS duplex is
233 also important for the efficient binding of JEV NS5Pol to its 5' end RNA (*Figure 6 - figure*
234 *supplement 1*), suggesting that the function of UFS in viral RdRp recruitment is conserved
235 among flaviviruses.

236 Next, *in vitro* RdRp assays using 5'-160 nt RNA as a template were performed to
237 investigate whether the role of the UFS in NS5Pol recruitment is required for *de novo* RNA
238 synthesis (*Figure 6D*). Apparently fewer products were generated in the reactions
239 containing templates with disrupted UFS elements compared with the reaction containing
240 the 5'-160 nt WT template, and restoration of the UFS duplex greatly increased the
241 amounts of RdRp products in reactions using the corresponding 5'-160 nt mutants as
242 templates. Moreover, an electrophoretic mobility shift assay (EMSA) experiment using
243 5'-160 nt RNA as a probe confirmed the function of UFS in NS5Pol recruitment, although
244 the overall affinity of 5'-160 nt RNA for NS5Pol was lower than that of 5'-300 nt RNA
245 (*Figure 6E*). Taken together, the above results demonstrated that the duplex conformation
246 of the UFS element is required for efficient NS5 recruitment and *de novo* initiation

247 efficiency, which is closely correlated with its function in vRNA replication.

248 **The stability of the UFS duplex determines its function in vRNA replication**

249 The UFS elements were shown to be rich in UA/AU base pairs, which contribute less to
250 the stability of RNA structures than CG/GC base pairs. Furthermore, internal loops and/or
251 wobble base pairs are prevalent inside the UFS or at the junction connecting the UFS and
252 SLB, which further decreases their structural stability. To investigate whether the low
253 stability of the UFS duplex is associated with its function, UA base pairs of the DENV4
254 UFS were progressively substituted with GC base pairs, and the replication efficiency of
255 the corresponding mutants was assessed using the above replicon system in BHK-21
256 cells (*Figure 7*). As expected, all mutants containing disrupted UFS elements showed only
257 extremely low levels of replication (*Figure 7. M2A, M2B, M4A and M4B*). One single
258 UA-to-GC substitution at different positions (*Figure 7. M2C1 and M2C2*) had little effect on
259 vRNA replication, in agreement with the above results (*Figure 3. M1C*). Surprisingly, all
260 UFS mutants containing 2 or more UA-to-GC base pair substitutions replicated poorly
261 compared with the WT replicon (*Figure 7, M2C and M4C*). In contrast, the M5 mutant
262 series, in which only one UA-to-GC substitution was involved, exhibited replication
263 characteristics similar to the M1 and M3 series. The above results indicated that
264 increasing the stability of the UFS duplex is harmful for vRNA replication.

265 To further confirm this finding and rule out the possibility that the base pair composition
266 itself affects UFS function, another panel of replicon mutants, which targeted the 3-nt
267 internal loop region between the DENV4 UFS and SLB, was generated. Shortening the
268 length of the internal loop to 1 nt or 2 nt did not affect vRNA replication greatly. In contrast,

total deletion of the internal loop, which caused the SLB to stack onto the UFS, significantly reduced the vRNA replication efficiency (*Figure 7 and Figure 7 - figure supplement 1, L1D, L2D and L3D*). Moreover, replication assays performed for various purine-to-purine and purine-to-pyrimidine substituting mutations targeting the internal loop (*Figure 7 - figure supplement 1*) suggested that the purine-rich properties of the internal loop are optimal for efficient DENV4 vRNA replication. Taken together, the above results demonstrated that the stability of the UFS duplex is a critical determinant for its function in vRNA replication. The defects in the vRNA replication of the over-stabilized UFS mutants were not caused by alternations in their affinity for NS5Pol, as an EMSA indicated that the 5'-300 nt M2C RNA bound to NS5Pol efficiently (*Figure 7 - figure supplement 2*).

Over-stabilized UFS hinders genome cyclization

RNA structure prediction (*Figure 1 - figure supplement 1 and Supplementary file 1*) and a previous report (*Sztuba-Solinska et al., 2013*) suggested that the UFS duplex is melted after genome cyclization, whereas the 5' UAR/SLB element, which is locked by the UFS duplex, is important for flavivirus genome cyclization (*Alvarez et al., 2005; Zhang et al., 2008*). We speculated that an over-stabilized UFS duplex would be too difficult to unwind and would hinder 5'-3' UAR hybridization. To confirm this probability, a 5'-3' RNA binding assay was employed (*Figure 8A*). The M1A, M1B and M1C mutations (*Figure 8B*), as well as the M3 series mutations (*Figure 8 - figure supplement 1*), had little effect on the formation of 5'-3' complex. However, when the M2 series mutants were assayed, although the M2A and M2B mutations also did not influence the formation of 5'-3' RNA complex apparently, the complex formed by the 3' UTR and 5'-300 nt M2C RNA was greatly

291 reduced compared to the amounts of complexes formed by the 3' UTR and other 5'-300 nt
292 RNA species (*Figure 8B*). Estimation of dissociation constant (*Figure 8 - figure*
293 *supplement 2*) revealed that the K_d of 5'-300 nt M2C binding with 3' UTR is approximately
294 10-fold higher than the K_d s of the other 5' RNAs. These results together indicated that
295 increasing the stability of the UFS hinders vRNA terminus interactions. Furthermore, the
296 5'-300 nt L3D mutant, in which the internal loop was deleted, also interacted with the 3'
297 UTR poorly (*Figure 8 - figure supplement 1*).

298 SHAPE analysis was then performed to observe the structural changes to 5' end RNA
299 caused by different concentrations of 3' UTR RNA (*Figure 9*). When the 5':3' ratio was 1:1,
300 the SHAPE reactivity of the UFS element in 5'-300 nt WT RNA exhibited a significant
301 increase compared with the reactivity when the 3' UTR was absent, and the SHAPE
302 reactivity of the SLB loop and 5' CS region was obviously reduced. When the 3' UTR was
303 in 5-fold excess of 5'-300 nt RNA, the SLB loop region of WT 5' RNA showed essentially
304 no SHAPE reactivity, indicating a complete transition from the SLB structure to a UAR
305 duplex. In contrast, when the 5'-300 nt M2C RNA was incubated with an equal
306 concentration of 3' UTR RNA, there were only minor changes in the SHAPE reactivity of
307 the UFS and SLB loop regions compared with those of 5'-300 nt M2C RNA alone. When
308 the 5':3' ratio was 1:5, the SLB loop region of 5'-300 nt M2C RNA still showed moderate
309 SHAPE reactivity. The above results demonstrated that the UFS duplex is melted when
310 the 3' UTR binds to 5' end RNA, and stabilization of the UFS renders it difficult to unwind
311 in response to the 3' UTR and thus hinders genome cyclization. Thus, although the UFS
312 does not participate in 5'-3' hybridization directly, the stability of its secondary structure

313 must be maintained below a threshold to enable the necessary conformational changes
314 required for genome cyclization. It can be speculated that the unwinding of the UFS during
315 genome cyclization may be important for its function in viral RNA synthesis.

316 **Genome cyclization reduces the affinity of NS5 for vRNA by inducing the unwinding**
317 **of the UFS**

318 As the UFS duplex is unwound after genome cyclization, it should not functionalize on
319 circularized genomes. To investigate this inference, artificial mini-genomes (*Figure 10A*),
320 which have been widely used in studies of flavivirus vRNA synthesis, RdRp activity and
321 RNA structures (*Niyomrattanakit et al., 2015; Potisopon et al., 2014; Sztuba-Solinska et*
322 *al., 2013; You and Padmanabhan, 1999*), were employed. The DENV4 WT mini-genome
323 and those containing the desired mutations were constructed (*Figure 10A*). First, using
324 native PAGE, we found that the WT mini-genome, as well as the M1A, M1B, M1C, M3A,
325 M3B, M3C and M2A mini-genomes, existed mostly in a circularized conformation (*Figure*
326 *10B*), whereas the CS-M mutant, in which the 5' CS sequence was mutated, was confined
327 to a linear conformation, as expected. The M2C mutant also mainly stayed in a linear
328 conformation, agreeing with the results of the 5'-3' RNA binding assay. The above results
329 demonstrated that these corresponding mini-genomes are highly circularized; thus, it is
330 unlikely that the UFS duplex structure exists in them. Next, the affinity of different
331 mini-genomes for NS5Pol was assessed. The WT, M1A, M1B and M1C mini-genomes all
332 showed low levels of binding to NS5Pol (*Figure 10C*). In contrast, the CS-M mini-genome
333 bound to NS5Pol with apparently higher affinity than the other mini-genomes tested
334 (*Figure 10C*).

335 Next, an *in vitro* RdRp assay was performed using mini-genomes as templates. The
336 CS-M mini-genome, together with a mini-genome lacking the SLA element (Δ SLA) or with
337 a disrupted cHP structure (cHP-M), were assayed in parallel as controls, which showed
338 non-detected or reduced RdRp activity for *de novo* initiation (*Figure 10D*), in agreement
339 with their known defects in vRNA replication. The *de novo* products in reactions using M1
340 and M3 series mini-genomes as templates were also all reduced compared to those
341 produced using the WT mini-genome as a template suggesting that the UFS is disabled in
342 mini-genomes because of unwinding of its duplex (*Figure 10D*). The differences in RdRp
343 activity between WT mini-genome and the UFS mutants were likely caused by changes of
344 primary sequence in these constructs, In supporting of this, the M1C and M3C mutants
345 were not able to reach the same level of replication as WT in replicon assay (*Figure 3D*),
346 and it has been reported that the base composition of U-rich sequence in the UFS was
347 actually able to affect vRNA replication of DENV2 (*Friebe and Harris, 2010*). Taken
348 together, the above results demonstrated that genome cyclization disables the function of
349 the UFS in NS5Pol recruitment, suggesting that the UFS has to function dynamically
350 during vRNA replication. Moreover, the attenuation of the affinity of NS5Pol for vRNA by
351 genome cyclization is potentially important for the translocation of NS5Pol from the 5' end
352 to the 3' end of vRNA.

353 **Mechanistic model for the function of the UFS in flavivirus replication**

354 It has been suggested that both the linear and circular conformations of the flavivirus
355 genome are required for vRNA replication and exist in equilibrium (*Villordo et al., 2010*).
356 However, circular states should be dominant among its conformations. Although the highly

357 circularized mini-genome is much shorter than the actual viral genome, it has been
358 theoretically proposed that the generic properties of a large RNA molecule lead its two
359 ends to stay close to each other (Yoffe *et al.*, 2011), which was supported by results from
360 single-molecule FRET assays (Leija-Martinez *et al.*, 2014). Thus, the 5' and 3' ends of the
361 flavivirus genome have great opportunities to contact each other, and due to the high
362 affinity between them, most vRNA molecules would stay circularized in the equilibrium
363 state. Moreover, protein factors have been shown to facilitate the cyclization of mRNA *and*
364 vRNA *in vivo* (Souii *et al.*, 2015; Wang *et al.*, 2011; Wells *et al.*, 1998). In fact, the PABP
365 protein, which bridges mRNA ends through poly(A)-PABP-eIF4E-5' cap interactions, has
366 been shown to bind to the DENV 3' UTR (Polacek *et al.*, 2009). However, if the linear
367 conformation of vRNA, the only conformation under which the UFS can exist, is present in
368 low abundance, the question remains of how the latter can function.

369 Inspired by the co-transcriptional folding of RNA molecules (Frieda and Block, 2012;
370 Gong *et al.*, 2015; Meyer and Miklos, 2004; Perdrizet *et al.*, 2012), we speculated that the
371 UFS duplex is folded during the ongoing synthesis of nascent positive-strand RNA
372 because the 5' end of the parental (+) strand is released from the dsRNA replication form
373 (RF) by a potential strand-displacement mechanism during the process, given that the
374 flavivirus genus exhibits semi-conservative replication (Chu and Westaway, 1985; Uchil
375 and Satchidanandam, 2003), whereas the 3' end of the parental (+) strand RNA remains
376 in double-stranded form with the (-) strand.

377 Based on the above considerations, we proposed that the UFS functions as an RNA
378 switch, and its "ON" and "OFF" states are controlled by genome cyclization (Figure 11) to

379 fulfill different needs in vRNA replication. A mechanistic model to explain the function of
380 the UFS is described below. (i) vRNA released in the cytoplasm is translated to generate a
381 sufficient level of viral proteins, which leads to the eventual binding of NS5 to the SLA and
382 the initiation of (-) strand synthesis, even without the presence of the UFS duplex. (ii)
383 Completion of (-) strand synthesis generates the dsRNA RF, which serves as the template
384 for the synthesis of progeny vRNA in the presence of viral NS5/NS3 and other viral/host
385 factors (not shown in *Figure 11*). (iii) During the elongation of the nascent (+) strand, the 5'
386 terminus of the parental (+) strand RNA is displaced first, and the UFS duplex is folded on
387 the protruding 5' end; this "ON" state of the UFS facilitates the recruitment of NS5 to the
388 free 5' end. (iv) After the completion of the nascent chain synthesis, the NS5-bound vRNA
389 undergoes genome cyclization, and the UFS element is set to "OFF" by the hybridization
390 between genome termini, which decreases the binding strength of NS5 to the 5' terminus
391 and promotes its translocation to the 3' terminus to initiate next-round synthesis of
392 negative-strand vRNA. Such dynamic modulation of NS5 binding should be of great
393 significance to maintain an appropriate level of (-) vRNA synthesis to ensure the global
394 balance of vRNA replication because the dsRNA RF is a highly active template for (+)
395 vRNA synthesis.

396 Furthermore, this RNA-switching mechanism is likely to be universal among
397 flaviviruses with vertebrate hosts given that when the terminal secondary structures of
398 both genome conformations of different flaviviruses were examined, we found that the 5'
399 local structures immediately following the SLA elements were always melted in response
400 to genome cyclization (*Figure 12 and Figure 12 - figure supplements 1-4*), suggesting that

401 these structures may possibly possess the same regulatory function as the UFS.

402 **Discussion**

403 Herein, via the combination of bioinformatics, biochemical and reverse genetics
404 approaches, the UFS element was shown to be crucial for efficient flavivirus vRNA
405 replication through dynamic modulation of viral RdRp recruitment. Our results
406 demonstrated that the UFS links two events of vRNA replication, NS5 recruitment and
407 genome cyclization, together, and the structural stability of the UFS is elaborately
408 balanced to meet the requirements of both. Especially, the conformational change of the
409 UFS caused by genome cyclization is coupled with its function in modulating dynamic
410 RdRp recruitment. As the function of UFS in viral replication and RdRp recruitment was
411 investigated using different flaviviruses (DENV4, JEV and ZIKV), it is plausible to consider
412 that the UFS is a general regulatory strategy of viral replication among the flavivirus genus.
413 Although a previous report (*Filomatori et al., 2011*) has suggested that the UFS may not
414 be functional in DENV2, this was more likely to be an exception, as our SHAPE data also
415 indicated that the UFS in DENV2 is highly unstable *in vitro*, in contrast to the UFS
416 elements from other viruses (*Figure 2*).

417 By applying a systemic RNA structure prediction and comparison approach covering
418 different members of the flavivirus genus, the structure of the downstream SLA region in
419 the 5' end of the flavivirus genome was unambiguously illuminated. The UA-base-pair-rich
420 UFS and the UFS-like element have been identified in MBFVs, two clades of NKVs, and
421 ISFVs, demonstrating that the UFS element is evolutionarily conserved. Interestingly,
422 while the UFS duplex unwinds during genome cyclization in MBFVs and NKVs, neither the

423 conserved mode of genome cyclization nor the unwinding of UFS-like elements during this
424 process was found in ISFVs. The ISFVs have been indicated to be the most divergent
425 outgroup among the genus flavivirus (*Blitvich and Firth, 2015; Cook and Holmes, 2006;*
426 *Moureaux et al., 2015*), which led us to assume that modern flaviviruses are evolved from
427 an insect virus ancestor. We speculated that primordial UFS-like structures are potential
428 viral replication enhancers with RdRp-recruiting functions in ancient ISFVs. When the
429 viruses were introduced into vertebrates, the intense selection pressure caused by shifting
430 between two hosts promoted the emergence of a highly efficient genome cyclization
431 strategy, and the UFS-like elements evolved into the RNA switches in modern flaviviruses.
432 Moreover, although the UFS structure itself was lost when the ancestral ISFV adapted into
433 ticks and some special vertebrates, its functional mechanism was inherited by the
434 appearance of elements such as 5'-SL2/CS-A in TBFVs. Thus, by looking into the
435 evolutionary history of flaviviruses and exploring the modes of genome cyclization among
436 them, we propose that the UFS may play a critical role during the evolution of the genus
437 flavivirus.

438 UFS elements usually localize close to, or overlap with, the translation start region,
439 suggesting a possible role for the UFS in viral translation regulation. Moreover, the
440 replication of most positive-strand RNA viruses occurs in virus-induced membrane
441 structures (*Gillespie et al., 2010; Welsch et al., 2009*). It is possible that during (+) vRNA
442 synthesis of flaviviruses, the parental (+) RNA is anchored to the vesicle membranes and
443 prevented from being transported out of the vesicle through interactions between the
444 UFS-containing 5' end and the membrane-bound viral replicase. Interestingly, DENV has

445 been reported to conceal its dsRNA in membrane structures to escape from host immunity
446 surveillance (*Uchida et al., 2014*). Thus, other potential functions of the UFS need further
447 investigation.

448 Functional long-range interactions are likely to be a general mechanism in
449 positive-strand RNA viruses (*Nicholson and White, 2014*). Genome cyclization is
450 responsible for the delivering of viral replication factors that bind 5'-terminally or internally
451 to the very 3' end of the viral genome. Such tactics have been observed in positive-strand
452 RNA viruses, which infect animals, plants and bacteria (*Nicholson and White, 2014*).
453 However, to our knowledge, this is the first report describing that an RNA switch triggered
454 by genome cyclization integrates the recruitment and translocation of the viral RdRp into
455 the dynamic process of nascent RNA synthesis. This deliberate control mechanism used
456 by flaviviruses could also be used by other positive-strand RNA viruses in similar forms,
457 and further pursuit of these mechanisms will provide deeper insight into the replication
458 and evolution of positive-strand RNA viruses.

459 **Materials and methods**

460 **DNA constructs**

461 The p4 infectious clone (*Durbin et al., 2001*) of the DENV4 814669 strain and its host *E.*
462 *coli* strain BD1528 were kindly provided by Professor Stephen S. Whitehead. All replicon
463 constructs were also manipulated using BD1528. The p4-Dualstop-SP-IRES-Rluc-Rep
464 replicon was generated by introducing a nonsense mutation into the 26th codon of the
465 capsid ORF (CAA to TAA) in the background of p4-CHPstop-SP-IRES-Rluc-Rep (*Liu et al.,*
466 *2013*). p4-Dualstop-SP-IRES-Rluc-Rep-GVD, in which the NS5 catalytic triad was

467 mutated, was generated based on p4-CHPstop-SP-IRES-Rluc-Rep-GVD using similar
468 strategies.

469 For the convenience of introducing mutations into the UFS region, the Asc I-SnaB I
470 fragment from p4-Dualstop-SP-IRES-Rluc-Rep, which contained the SP6 promoter region
471 and the DENV4 5' UTR-capsid ORF sequence, was engineered such that the sequence
472 corresponding to the 70-107 nt region of the DENV4 genome was substituted by the
473 following: 5'- CTCCTCACACATACGTAATGGGGGAGGAG-3'. This engineered fragment
474 contained two inversely positioned BseR I sites (underlined above) and was cloned into
475 pGEM-T easy (Promega, Madison, Wisconsin) to generate the cloning cassette vector,
476 pBseRI-Dualstop-04. DNA oligos containing the desired mutations of the UFS were
477 annealed and ligated with BseR I-digested pBseRI-Dualstop-04 to acquire Asc I-SnaB I
478 fragments with the desired mutations, which were then subcloned back into
479 p4-Dualstop-SP-IRES-Rluc-Rep.

480 To generate UFS mutants in the p4 infectious clone and p4-GVD, the Asc I-BstE II
481 fragments with desired mutations were generated by overlapping PCR using the
482 corresponding replicon mutants and p4 infectious clone DNA as templates for
483 amplification, cloned into pGEM-T easy, and then subcloned into p4 and p4-GVD,
484 respectively.

485 Site-directed mutagenesis method was employed for the generation of ZIKV fragments
486 containing the desired UFS mutations, the generated Not I-Avr II restriction fragments
487 were then subcloned into the infectious clone of ZIKV strain FSS13025 (*Shan et al., 2016*),
488 which was kindly provided by Professor Pei-Yong Shi.

489 The DENV4 mini-genomes were constructed by joining various 5'-300 nt fragments
490 with the 3' UTR sequence using overlapping PCR techniques. The mutations targeting
491 cHP and 5'CS were also introduced by overlapping PCR.

492 The DENV2 and DENV3 5' end sequences were acquired by RT-PCR using the
493 DENV2 strain NGC (KM204118) and the DENV3 strain 80-2 (AF317645) RNA as
494 templates respectively, and cloned into pMD-19T-simple (Takara, Dalian, China). The 5'
495 end sequence of DENV1 strain WestPac (U88535) was chemically synthesized and
496 cloned into pUC57 by Thermo Fisher Scientific. The SP6 promoter sequence was placed
497 upstream of the DENV1 5' end sequence. These constructs, together with the JEV
498 infectious clone pAJE70 (*Li et al., 2013*), which contains the 5' UTR-C-coding region of
499 strain SA-14-14-2 (AF315119), were utilized to amplify the DNA templates for *in vitro*
500 transcription. The infectious clone of ZIKV strain FSS13025 was used to amplify the DNA
501 template for *in vitro* transcription of ZIKV 5' end RNA. JEV UFS mutants were generated
502 by site-directed mutagenesis, the resultant plasmids were utilized to amplify the DNA
503 templates for *in vitro* transcription of the corresponding JEV 5' RNA mutants.

504 **RNA preparation**

505 Replicon and full-length viral RNA were *in vitro* transcribed as described previously (*Liu*
506 *et al., 2013*). To generate RNA species for *in vitro* SHAPE, EMSA and RdRp activity
507 assays, high-fidelity PCR-amplified DNA fragments, which contained the SP6 promoter,
508 were used as templates for *in vitro* transcription reactions. RNA was purified with an
509 RNeasy mini kit (Qiagen, Hilden, Germany), and the concentrations were determined
510 spectrophotometrically. Agarose/TAE gel electrophoresis was routinely conducted to

511 examine the integrity of the purified RNA. The RNA preparations were stored at -80 °C
512 before use. Note that all DENV4 5' RNA and mini-genome RNA molecules contained two
513 artificial nonsense mutations at the corresponding sites in the capsid coding region that
514 have been shown not to affect the folding of the corresponding RNA or vRNA replication
515 (*Clyde et al., 2008; Liu et al., 2013*).

516 **Replicon assay**

517 For the evaluation of the replication characteristics of the
518 p4-CHPstop-SP-IRES-Rluc-Rep and p4-Dualstop-SP-IRES-Rluc-Rep replicons, a replicon
519 assay was performed as described previously (*Liu et al., 2013*). For the replicon assays of
520 the UFS mutants, ten thousand BHK-21 cells were seeded into each well of Nunc
521 MicroWell 96-Well Optical-Bottom Plates (Thermo Fisher Scientific, Waltham,
522 Massachusetts) one day prior to transfection. Unless otherwise specified, 100 ng of
523 replicon RNA was transfected per well using Lipofectamine 2000 reagent (Thermo Fisher
524 Scientific, Waltham, Massachusetts), and the plates were cultured at 37 °C with 5% CO₂.
525 At the indicated time points, the cells in the microplates were lysed with 1× *Renilla* lysis
526 buffer (Promega, Madison, Wisconsin) and stored at -20 °C until use. The *Renilla*
527 luciferase activity of the collected samples was measured as described previously (*Liu et*
528 *al., 2013*), except that the microplates were directly subjected to the GloMax-96
529 luminometer.

530 **Electroporation of full-length vRNA, qRT-PCR and virus titration**

531 Four million BHK-21 cells suspended in 400 µl of Opti-MEM I medium were
532 electroporated with 5 µg of vRNA. The details of the electroporation are described

533 elsewhere (*Liu et al., 2013*). The electroporated cells were resuspended in 14 ml of
534 Dulbecco's modified minimal essential medium (DMEM, Thermo Fisher Scientific,
535 Waltham, Massachusetts) with 5% fetal bovine serum (FBS, PAA, Morningside, QLD,
536 Australia) and dispensed into 24-well plates with or without sterile cover slips. The cells
537 were cultured at 37 °C in 5% CO₂. At 4 h post-electroporation, a media change was
538 performed for the plates intended for vRNA quantification analysis. At the indicated time
539 points, the total RNA was isolated from the transfected cells, and qRT-PCR was
540 performed to quantify vRNA copies as described previously (*Liu et al., 2013*). The culture
541 supernatants from the transfected cells were collected at different time points
542 post-transfection, and virus titers were determined by plaque-forming assays.

543 **Indirect immunofluorescence assay**

544 BHK-21 cells electroporated with corresponding vRNA were seeded onto cover slips in
545 24-well plate-format and cultured at 37 °C in 5% CO₂. At the indicated time points, the
546 cover slips were washed once with PBS (phosphate buffered saline, pH 7.4) and fixed
547 with acetone/methanol (v/v: 3/7) at 4 °C. The cover slips were incubated with the
548 anti-dengue envelope protein monoclonal antibody 2A10G6 at 37 °C for 1 h for the cells
549 transfected with DENV4 RNA, and anti-ZIKV envelope protein mAb clone 0302156
550 (1:1000 diluted, BioFront Technologies, Tallahassee, Florida, USA) was used for the cells
551 transfected with ZIKV RNA. After the incubation with primary antibodies, the cover slips
552 were washed with PBS for three times. AlexaFluor 488-labeled goat anti-mouse IgG
553 (1:200 diluted, zsbio, Beijing, China) was then added, and after a 1-h incubation, the cover
554 slips were washed as described above. For cell nuclei staining, 4',

555 6-diamidino-2-phenylindole (DAPI, 0.5 ng/μl) was added onto the cover slips and
556 incubated for 5 min. An Olympus BX51 microscope under the control of DP72 software
557 was utilized for image capture.

558 **SHAPE analysis**

559 RNA molecules (approximately 9.66 pmol) corresponding to the WT or mutated 5' end
560 sequence of different flaviviruses was refolded in an 18-μl reaction and then modified by
561 N-methylisatoic anhydride (NMIA, Sigma-Aldrich, St. Louis, Missouri). For the analysis of
562 5' end RNA-3' UTR complexes, the two RNA segments were co-folded at the indicated
563 molar ratios and then subjected to NMIA modification. The modified RNA was purified
564 using RNA Clean & Concentrator-5 (Zymo Research, Irvine, California, USA). Primer
565 extension reactions utilizing fluorophore-labeled primers were performed with Superscript
566 II reverse transcriptase (Thermo Fisher Scientific, Waltham, Massachusetts) in a 20-μl
567 volume according to the manufacturer's instructions. ddTTP dideoxy-sequencing
568 reactions were performed in parallel. We routinely used VIC-labeled primers for primer
569 extension of the SHAPE reactions and NED-labeled primers for sequencing reactions.
570 Otherwise, FAM- and HEX-labeled primers were utilized for primer extension of the
571 SHAPE and sequencing reactions, respectively. After primer extension, one microliter of 4
572 M NaOH was added to each reaction, and treatment at 95 °C for 3 min was performed to
573 hydrolyze the RNA templates. Two microliters of 2 M HCl were added to adjust the pH to
574 neutral. Then, the sequencing reactions were split and added into the SHAPE (+) and (-)
575 reactions. The final mixtures were purified by ethanol/EDTA precipitation, dissolved in
576 Hi-Di formamide and separated via denaturing PAGE capillary electrophoresis by the DNA

577 sequencing department of Thermo Fisher Scientific. The SHAPE data were analyzed
578 using QuShape software (*Karabiber et al., 2013*). All the processing steps were performed
579 using the default software settings. Negative SHAPE reactivity was set to zero expect for
580 the calculations of the Δ SHAPE reactivity of WT and M2C 5'-300 nt RNA in response to 3'
581 UTR RNA.

582 **Expression and purification of recombinant DENV4/JEV NS5Pol**

583 The coding sequence of the DENV4 NS5 RdRp domain (residues 270-900, NS5Pol)
584 was cloned into a pET-28a (+) expression vector using Nhe I/Xho I restriction sites. The
585 recombinant NS5Pol carrying an N-terminal His-tag was expressed in *E. coli* Rosetta
586 (λ DE3) in the presence of 0.125 mM isopropyl- β -D-thiogalactopyranoside (IPTG) at 16 °C
587 for 20 h. The cell pellets were harvested and washed once with Buffer A (25 mM Tris.Cl,
588 pH 8.0, 500 mM NaCl, 25 mM imidazole and 5% glycerol) and resuspended in Buffer A
589 containing cOmplete EDTA-free protease inhibitor cocktail tablets (Roche, Penzberg,
590 Germany). After ultra-sonication, the suspension was centrifuged at 30,000 g at 4 °C for
591 20 min. The soluble recombinant NS5Pol protein in the supernatants was then purified
592 using a HisTrap HP column (GE Healthcare, Little Chalfont, UK). The fraction containing
593 NS5Pol was eluted with Buffer A containing 300 mM imidazole. The eluted protein was
594 exchanged into 50 mM Tris.Cl (pH 8.0), 300 mM NaCl and 20% glycerol using a HiTrap
595 desalting column (GE Healthcare, Little Chalfont, UK) and concentrated to mg/ml grade by
596 ultrafiltration using Amicon Ultra-15 Centrifugal Filter Units (30 kDa-cutoff, Merck Millipore,
597 Billerica, Massachusetts, USA). Dithiothreitol (DTT) was added into the purified NS5Pol
598 protein to a final concentration of 1 mM. The final product was dispensed into single-use

599 aliquots and stored at -80 °C before use. NS5Pol of JEV SA-14-14-2 strain was cloned,
600 expressed and purified using the same strategy.

601 **EMSA assay**

602 An RNA-RNA binding EMSA was performed as described previously (*Liu et al., 2013*)
603 with minor modifications. For the NS5Pol-RNA EMSA assays, the different DENV4 5'-300
604 nt RNA species were first diluted in 0.5× TE buffer and heated at 95 °C for 2 min. The RNA
605 samples were then placed on ice immediately. 5× RNA folding buffer T (250 mM Tris.Cl,
606 pH 8.0, 500 mM NaCl and 25 mM MgCl₂) was added to the samples, and the RNA was
607 refolded at 37 °C for 20 min. The concentration of the renatured RNA was set to 500 nM.
608 The binding reactions contained 50 nM 5'-300 nt RNA, 4 µl of 5× EMSA buffer (200 mM
609 Tris.Cl, pH 8.0, 300 mM NaCl, 25 mM MgCl₂), 0.05 mg/ml heparin sodium salt, 7.5%
610 glycerol and different amounts of NS5Pol (0, 3, 5.25, 7.5 and 11.25 µg) in a 20-µl volume.
611 Due to the solvent components in RNA and protein preparations, the final reactions
612 contained 64.15 mM Tris.Cl (pH 8.0), 182.5 mM NaCl, 5.5 mM MgCl₂, 40 nM EDTA and
613 375 nM DTT. The reactions were incubated at 30 °C for 30 min, and then, 10× gel loading
614 solution (Thermo Fisher Scientific, Waltham, Massachusetts) was added, and the
615 mixtures were separated by electrophoresis on 6% native PAGE gels running in 0.5× TBE.
616 The gel apparatus was placed in an ice-water bath to prevent the dissociation of
617 RNA-protein complexes. After running at 60 V for 4 h, the gels were stained with SYBR
618 Gold nucleic acid gel stain (Thermo Fisher Scientific, Waltham, Massachusetts) for 30 min,
619 and gel pictures were captured using a BioSpectrum Imaging System (UVP, LLC, Upland,
620 California) with a UV transilluminator. EMSAs using 5'-160 nt RNA or mini-genome RNA

were performed similarly, with a few exceptions: for the 5'-160 nt RNA-based EMSA, the NS5Pol concentrations were higher (0, 5.4, 10.8, 16.2 and 21.6 µg, respectively); for the mini-genome-based EMSA, the heparin concentration was set to 0.16 mg/ml, and the electrophoresis was performed with 4.5% PAGE gels at 75 V for 6 h in an ice-water bath. EMSA assay using JEV NS5Pol and 5'-320 nt RNA was performed with similar conditions for DENV4 5'-300 nt RNA EMSA assay.

RdRp assay

In vitro RdRp initiation assays were performed using: (I) 5'-160 nt RNA of DENV4, (II) DENV4 mini-genome RNA as templates. The RNA templates were diluted with RNase-free water to a final volume of 8 µl, then heated at 95 °C for 2 min and immediately cooled on ice. Two microliters of RNA fold buffer T2 (250 mM Tris.Cl, pH 7.4, 100 mM NaCl, 25 mM MgCl₂) was added, and the RNA templates were folded at 37 °C for 20 min. Unless otherwise specified, the 30-µl RdRp reactions contained 450 ng of template RNA (3 µl of 150 ng/µl folded RNA), 55.6 mM Tris.Cl (pH 7.4), 12 mM NaCl, 5.5 mM MgCl₂, 2 mM MnCl₂, 10 mM DTT, 40 U of recombinant RNase inhibitor (40 U/µl), approximately 5.4 µg NS5Pol (in 1 µl) and 0.5 mM ATP, GTP, and UTP; 0.1 mM CTP; and 0.25 mM biotin-11-CTP (Roche, Penzberg, Germany). According to previous reports (*Ackermann and Padmanabhan, 2001; Filomatori et al., 2006*), the RdRp reactions were incubated at 30 °C for the desired length of time. The reaction products were purified using an RNAClean Kit (Tiangen, Beijing, China), and 2× RNA loading dye (New England Biolabs, Ipswich, Massachusetts) was added into the purified RNA. The samples were preheated at 70 °C for 5 min, snap-cooled on ice, and analyzed using 6% PAGE/8 M urea gels. The

643 gel-separated RNA was electro-transferred onto a Hybond N+ Nylon membrane (GE
644 Healthcare, Little Chalfont, UK). After air-drying the membrane, the transferred RNA was
645 UV-crosslinked by an UV transilluminator for 10 min. The membrane was blocked using
646 10% non-fat dry milk, and then streptavidin-conjugated HRP (Thermo Fisher Scientific,
647 Waltham, Massachusetts, USA) was incubated with the membrane at room temperature
648 for 2 h. The membrane was then extensively washed using PBS with 0.05% Tween 20,
649 and chemiluminescence signals were detected using a Pro-light chemiluminescent kit
650 (Tiangen, Beijing, China) and a Smartchemi II imaging system (Sage Creation Science Co,
651 Beijing, China).

652 **Statistical analysis**

653 Statistical analysis was performed using the statistical functions of GraphPad Prism 6
654 (GraphPad Software, La Jolla, California, USA). Briefly, Paired t-test was performed for
655 Figure 3B. One-way ANOVA and Dunnett's multiple comparisons test were performed for
656 Figure 2 - figure supplement 1, Figure 3D, Figure 4, Figure 7 and Figure 7 - figure
657 supplement 1. Two-way ANOVA and Tukey's multiple comparisons test were performed
658 for Figure 5B, 5C, 5D, 5F, 5G, 5H and 5I. The detailed results of statistical analysis were
659 provided within the corresponding source data files.

660 **Acknowledgement**

661 We appreciate Prof. Stephen S. Whitehead (National Institute of Allergy and Infectious
662 Diseases, NIH, USA) and Prof. Pei-Yong Shi (University of Texas Medical Branch, USA) for
663 the p4 infectious clone and the infectious clone of ZIKV strain FSS13025, respectively.
664 The authors thank Dr. Guang-Chuan Wang (Zhejiang University) for insightful comments

665 and discussions. This work was supported by the National Key Research and
666 Development Project of China (2016YFD0500304), the National Natural Science
667 Foundation of China (No. 31270196, 31000083 and 30972613) and National 973 project
668 of China (2012CB518904). CF Qin was supported by Excellent Young Scientist Program
669 from the National Natural Science Foundation of China (81522025) and the Newton
670 Advanced Fellowship from the UK Academy of Medical Sciences and NSFC (No.
671 81661130162).

672 **Author contributions**

673 ZYL designed and performed the experiments, acquired, analyzed and interpreted the
674 data, drafted and revised the article; XFL and TJ analyzed and interpreted the data;
675 YQD, QY, HZ and JYY performed the experiments and acquired the data; CFQ designed
676 the experiments, drafted and revised the article.

677 **References**

678 Ackermann M and Padmanabhan R. 2001. De novo synthesis of RNA by the dengue virus
679 RNA-dependent RNA polymerase exhibits temperature dependence at the initiation but
680 not elongation phase. *J Biol Chem* **276**: 39926–37. doi: 10.1074/jbc.
681 Alvarez DE, Lodeiro MF, Luduena SJ, Pietrasanta LI and Gamarnik AV. 2005. Long-range
682 RNA-RNA interactions circularize the dengue virus genome. *J Virol* **79**: 6631-43. doi:
683 10.1128/JVI.79.11.6631-6643.2005.
684 Athavale SS, Gossett JJ, Bowman JC, Hud NV, Williams LD and Harvey SC. 2013. In vitro
685 secondary structure of the genomic RNA of satellite tobacco mosaic virus. *PLoS One* **8**:
686 e54384. doi: 10.1371/journal.pone.0054384.

687 Blitvich BJ and Firth AE. 2015. Insect-specific flaviviruses: a systematic review of their
688 discovery, host range, mode of transmission, superinfection exclusion potential and
689 genomic organization. *Viruses* **7**: 1927-59. doi: 10.3390/v7041927.

690 Brierley I and Dos Ramos FJ. 2006. Programmed ribosomal frameshifting in HIV-1 and
691 the SARS-CoV. *Virus Res* **119**: 29-42. doi: 10.1016/j.virusres.2005.10.008.

692 Chapman EG, Moon SL, Wilusz J and Kieft JS. 2014. RNA structures that resist
693 degradation by Xrn1 produce a pathogenic Dengue virus RNA. *eLife* **3**: e01892. doi:
694 10.7554/eLife.01892.

695 Chiu WW, Kinney RM and Dreher TW. 2005. Control of translation by the 5'- and
696 3'-terminal regions of the dengue virus genome. *J Virol* **79**: 8303-15. doi:
697 10.1128/JVI.79.13.8303-8315.2005.

698 Chu PW and Westaway EG. 1985. Replication strategy of Kunjin virus: evidence for
699 recycling role of replicative form RNA as template in semiconservative and asymmetric
700 replication. *Virology* **140**: 68-79.

701 Clyde K, Barrera J and Harris E. 2008. The capsid-coding region hairpin element (cHP) is
702 a critical determinant of dengue virus and West Nile virus RNA synthesis. *Virology* **379**:
703 314-23. doi: 10.1016/j.virol.2008.06.034.

704 Clyde K and Harris E. 2006. RNA secondary structure in the coding region of dengue virus
705 type 2 directs translation start codon selection and is required for viral replication. *J Virol*
706 **80**: 2170-82. doi: 10.1128/JVI.80.5.2170-2182.2006.

707 Cook S and Holmes EC. 2006. A multigene analysis of the phylogenetic relationships
708 among the flaviviruses (Family: Flaviviridae) and the evolution of vector transmission.

709 *Arch Virol* **151**: 309-25. doi: 10.1007/s00705-005-0626-6.

710 de Borba L, Villordo SM, Iglesias NG, Filomatori CV, Gebhard LG and Gamarnik AV. 2015.

711 Overlapping local and long-range RNA-RNA interactions modulate dengue virus genome

712 cyclization and replication. *J Virol* **89**: 3430-7. doi: 10.1128/JVI.02677-14.

713 Dong H, Zhang B and Shi PY. 2008. Terminal structures of West Nile virus genomic RNA

714 and their interactions with viral NS5 protein. *Virology* **381**: 123-35. doi:

715 10.1016/j.virol.2008.07.040.

716 Durbin AP, Karron RA, Sun W, Vaughn DW, Reynolds MJ, Perreault JR, Thumar B, Men

717 R, Lai CJ, Elkins WR, Chanock RM, Murphy BR and Whitehead SS. 2001. Attenuation

718 and immunogenicity in humans of a live dengue virus type-4 vaccine candidate with a 30

719 nucleotide deletion in its 3'-untranslated region. *Am J Trop Med Hyg* **65**: 405-13.

720 Egloff MP, Benarroch D, Selisko B, Romette JL and Canard B. 2002. An RNA cap

721 (nucleoside-2'-O-)-methyltransferase in the flavivirus RNA polymerase NS5: crystal

722 structure and functional characterization. *EMBO J* **21**: 2757-68. doi:

723 10.1093/emboj/21.11.2757.

724 Fauci AS and Morens DM. 2016. Zika Virus in the Americas--Yet Another Arbovirus

725 Threat. *N Engl J Med* **374**: 601-4. doi: 10.1056/NEJMp1600297.

726 Filomatori CV, Iglesias NG, Villordo SM, Alvarez DE and Gamarnik AV. 2011. RNA

727 sequences and structures required for the recruitment and activity of the dengue virus

728 polymerase. *J Biol Chem* **286**: 6929-39. doi: 10.1074/jbc.M110.162289.

729 Filomatori CV, Lodeiro MF, Alvarez DE, Samsa MM, Pietrasanta L and Gamarnik AV.

730 2006. A 5' RNA element promotes dengue virus RNA synthesis on a circular genome.

731 *Genes Dev* **20**: 2238-49. doi: 10.1101/gad.1444206.

732 Friebe P and Harris E. 2010. Interplay of RNA elements in the dengue virus 5' and 3' ends
 733 required for viral RNA replication. *J Virol* **84**: 6103-18. doi: 10.1128/JVI.02042-09.

734 Friebe P, Shi PY and Harris E. 2011. The 5' and 3' downstream AUG region elements are
 735 required for mosquito-borne flavivirus RNA replication. *J Virol* **85**: 1900-5. doi:
 736 10.1128/JVI.02037-10.

737 Frieda KL and Block SM. 2012. Direct observation of cotranscriptional folding in an
 738 adenine riboswitch. *Science* **338**: 397-400. doi: 10.1126/science.1225722.

739 Funk A, Truong K, Nagasaki T, Torres S, Floden N, Balmori Melian E, Edmonds J, Dong
 740 H, Shi PY and Khromykh AA. 2010. RNA structures required for production of subgenomic
 741 flavivirus RNA. *J Virol* **84**: 11407-17. doi: 10.1128/JVI.01159-10.

742 Gebhard LG, Filomatori CV and Gamarnik AV. 2011. Functional RNA elements in the
 743 dengue virus genome. *Viruses* **3**: 1739-56. doi: 10.3390/v3091739.

744 Gillespie LK, Hoenen A, Morgan G and Mackenzie JM. 2010. The endoplasmic reticulum
 745 provides the membrane platform for biogenesis of the flavivirus replication complex. *J*
 746 *Viro* **84**: 10438-47. doi: 10.1128/JVI.00986-10.

747 Gong S, Wang Y and Zhang W. 2015. Kinetic regulation mechanism of pbuE riboswitch. *J*
 748 *Chem Phys* **142**: 015103. doi: 10.1063/1.4905214.

749 Goto H, Muramoto Y, Noda T and Kawaoka Y. 2013. The genome-packaging signal of the
 750 influenza A virus genome comprises a genome incorporation signal and a
 751 genome-bundling signal. *J Virol* **87**: 11316-22. doi: 10.1128/JVI.01301-13.

752 Issur M, Geiss BJ, Bougie I, Picard-Jean F, Despins S, Mayette J, Hobdey SE and

753 Bisailon M. 2009. The flavivirus NS5 protein is a true RNA guanylyltransferase that
 754 catalyzes a two-step reaction to form the RNA cap structure. *RNA* **15**: 2340-50. doi:
 755 10.1261/rna.1609709.

756 Karabiber F, McGinnis JL, Favorov OV and Weeks KM. 2013. QuShape: rapid, accurate,
 757 and best-practices quantification of nucleic acid probing information, resolved by capillary
 758 electrophoresis. *RNA* **19**: 63-73. doi: 10.1261/rna.036327.112.

759 Keane SC, Heng X, Lu K, Kharytonchik S, Ramakrishnan V, Carter G, Barton S, Hosic A,
 760 Florwick A, Santos J, Bolden NC, McCowin S, Case DA, Johnson BA, Salemi M,
 761 Telesnitsky A and Summers MF. 2015. RNA structure. Structure of the HIV-1 RNA
 762 packaging signal. *Science* **348**: 917-21. doi: 10.1126/science.aaa9266.

763 Khromykh AA, Meka H, Guyatt KJ and Westaway EG. 2001. Essential role of cyclization
 764 sequences in flavivirus RNA replication. *J Virol* **75**: 6719-28. doi:
 765 10.1128/JVI.75.14.6719-6728.2001.

766 Kieft JS. 2008. Viral IRES RNA structures and ribosome interactions. *Trends Biochem Sci*
 767 **33**: 274-83. doi: 10.1016/j.tibs.2008.04.007.

768 Klema VJ, Padmanabhan R and Choi KH. 2015. Flaviviral Replication Complex:
 769 Coordination between RNA Synthesis and 5'-RNA Capping. *Viruses* **7**: 4640-56. doi:
 770 10.3390/v7082837.

771 Leija-Martinez N, Casas-Flores S, Cadena-Nava RD, Roca JA, Mendez-Cabanas JA,
 772 Gomez E and Ruiz-Garcia J. 2014. The separation between the 5'-3' ends in long RNA
 773 molecules is short and nearly constant. *Nucleic Acids Res* **42**: 13963-8. doi:
 774 10.1093/nar/gku1249.

775 Li SH, Dong H, Li XF, Xie X, Zhao H, Deng YQ, Wang XY, Ye Q, Zhu SY, Wang HJ, Zhang
 776 B, Leng QB, Zuest R, Qin ED, Qin CF and Shi PY. 2013. Rational design of a flavivirus
 777 vaccine by abolishing viral RNA 2'-O methylation. *J Virol* **87**: 5812-9. doi:
 778 10.1128/JVI.02806-12.
 779 Liu Y, Wimmer E and Paul AV. 2009. Cis-acting RNA elements in human and animal
 780 plus-strand RNA viruses. *Biochim Biophys Acta* **1789**: 495-517. doi:
 781 10.1016/j.bbagr.2009.09.007.
 782 Liu ZY, Li XF, Jiang T, Deng YQ, Zhao H, Wang HJ, Ye Q, Zhu SY, Qiu Y, Zhou X, Qin ED
 783 and Qin CF. 2013. Novel cis-acting element within the capsid-coding region enhances
 784 flavivirus viral-RNA replication by regulating genome cyclization. *J Virol* **87**: 6804-18. doi:
 785 10.1128/JVI.00243-13.
 786 Lodeiro MF, Filomatori CV and Gamarnik AV. 2009. Structural and functional studies of the
 787 promoter element for dengue virus RNA replication. *J Virol* **83**: 993-1008. doi:
 788 10.1128/JVI.01647-08.
 789 Meyer IM and Miklos I. 2004. Co-transcriptional folding is encoded within RNA genes.
 790 *BMC Mol Biol* **5**: 10. doi: 10.1186/1471-2199-5-10.
 791 Mlakar J, Korva M, Tul N, Popovic M, Poljsak-Prijatelj M, Mraz J, Kolenc M, Resman Rus
 792 K, Vesnaver Vipotnik T, Fabjan Vodusek V, Vizjak A, Pizem J, Petrovec M and Avsic
 793 Zupanc T. 2016. Zika Virus Associated with Microcephaly. *N Engl J Med* **374**: 951-8. doi:
 794 10.1056/NEJMoa1600651.
 795 Morales L, Mateos-Gomez PA, Capiscol C, del Palacio L, Enjuanes L and Sola I. 2013.
 796 Transmissible gastroenteritis coronavirus genome packaging signal is located at the 5'

797 end of the genome and promotes viral RNA incorporation into virions in a
 798 replication-independent process. *J Virol* **87**: 11579-90. doi: 10.1128/JVI.01836-13.
 799 Moureau G, Cook S, Lemey P, Nougairede A, Forrester NL, Khasnatinov M, Charrel RN,
 800 Firth AE, Gould EA and de Lamballerie X. 2015. New insights into flavivirus evolution,
 801 taxonomy and biogeographic history, extended by analysis of canonical and alternative
 802 coding sequences. *PLoS One* **10**: e0117849. doi: 10.1371/journal.pone.0117849.
 803 Nicholson BL and White KA. 2014. Functional long-range RNA-RNA interactions in
 804 positive-strand RNA viruses. *Nat Rev Microbiol* **12**: 493-504. doi: 10.1038/nrmicro3288.
 805 Niyomrattanakit P, Wan KF, Chung KY, Abas SN, Seh CC, Dong H, Lim CC, Chao AT, Lee
 806 CB, Nilar S, Lescar J, Shi PY, Beer D and Lim SP. 2015. Stabilization of dengue virus
 807 polymerase in de novo initiation assay provides advantages for compound screening.
 808 *Antiviral Res* **119**: 36-46. doi: 10.1016/j.antiviral.2015.04.007.
 809 Nomaguchi M, Ackermann M, Yon C, You S and Padmanbhan R. 2003. De Novo
 810 Synthesis of Negative-Strand RNA by Dengue Virus RNA-Dependent RNA Polymerase In
 811 Vitro: Nucleotide, Primer, and Template Parameters. *J Virol* **77**: 8831-42. doi:
 812 10.1128/jvi.77.16.8831-8842.2003.
 813 Perdrietz GA, 2nd, Artsimovitch I, Furman R, Sosnick TR and Pan T. 2012. Transcriptional
 814 pausing coordinates folding of the aptamer domain and the expression platform of a
 815 riboswitch. *Proc Natl Acad Sci U S A* **109**: 3323-8. doi: 10.1073/pnas.1113086109.
 816 Polacek C, Friebe P and Harris E. 2009. Poly(A)-binding protein binds to the
 817 non-polyadenylated 3' untranslated region of dengue virus and modulates translation
 818 efficiency. *J Gen Virol* **90**: 687-92. doi: 10.1099/vir.0.007021-0.

819 Potisopon S, Priet S, Collet A, Decroly E, Canard B and Selisko B. 2014. The
820 methyltransferase domain of dengue virus protein NS5 ensures efficient RNA synthesis
821 initiation and elongation by the polymerase domain. *Nucleic Acids Res* **42**: 11642-56. doi:
822 10.1093/nar/gku666.

823 Reuter JS and Mathews DH. 2010. RNAstructure: software for RNA secondary structure
824 prediction and analysis. *BMC Bioinformatics* **11**: 129. doi: 10.1186/1471-2105-11-129.

825 Roby JA, Pijlman GP, Wilusz J and Khromykh AA. 2014. Noncoding subgenomic flavivirus
826 RNA: multiple functions in West Nile virus pathogenesis and modulation of host
827 responses. *Viruses* **6**: 404-27. doi: 10.3390/v6020404.

828 Rouha H, Hoenninger VM, Thurner C and Mandl CW. 2011. Mutational analysis of three
829 predicted 5'-proximal stem-loop structures in the genome of tick-borne encephalitis virus
830 indicates different roles in RNA replication and translation. *Virology* **417**: 79-86. doi:
831 10.1016/j.virol.2011.05.008.

832 Shan C, Xie X, Muruato AE, Rossi SL, Roundy CM, Azar SR, Yang Y, Tesh RB, Bourne N,
833 Barrett AD, Vasilakis N, Weaver SC and Shi PY. 2016. An infectious cDNA clone of Zika
834 virus to study viral virulence, mosquito transmission, and antiviral inhibitors. *Cell Host &*
835 *Microbe* **19**: 891–900. doi: 10.1016/j.chom.2016.05.004.

836 Shetty S, Stefanovic S and Mihailescu MR. 2013. Hepatitis C virus RNA: molecular
837 switches mediated by long-range RNA-RNA interactions? *Nucleic Acids Res* **41**: 2526-40.
838 doi: 10.1093/nar/gks1318.

839 Simon AE and Miller WA. 2013. 3' cap-independent translation enhancers of plant viruses.
840 *Annu Rev Microbiol* **67**: 21-42. doi: 10.1146/annurev-micro-092412-155609.

841 Souii A, M'Hadheb-Gharbi MB and Gharbi J. 2015. Cellular Proteins Act as Bridge
842 Between 5' and 3' Ends of the Coxsackievirus B3 Mediating Genome Circularization
843 During RNA Translation. *Curr Microbiol* **71**: 387-95. doi: 10.1007/s00284-015-0866-y.
844 Sztuba-Solinska J, Teramoto T, Rausch JW, Shapiro BA, Padmanabhan R and Le Grice
845 SF. 2013. Structural complexity of Dengue virus untranslated regions: cis-acting RNA
846 motifs and pseudoknot interactions modulating functionality of the viral genome. *Nucleic*
847 *Acids Res* **41**: 5075-89. doi: 10.1093/nar/gkt203.
848 Tsetsarkin KA, Liu G, Shen K and Pletnev AG. 2016. Kissing-loop interaction between 5'
849 and 3' ends of tick-borne Langat virus genome 'bridges the gap' between mosquito- and
850 tick-borne flaviviruses in mechanisms of viral RNA cyclization: applications for virus
851 attenuation and vaccine development. *Nucleic Acids Res*. doi: 10.1093/nar/gkw061.
852 Uchida L, Espada-Murao LA, Takamatsu Y, Okamoto K, Hayasaka D, Yu F, Nabeshima T,
853 Buerano CC and Morita K. 2014. The dengue virus conceals double-stranded RNA in the
854 intracellular membrane to escape from an interferon response. *Sci Rep* **4**: 7395. doi:
855 10.1038/srep07395.
856 Uchil PD and Satchidanandam V. 2003. Characterization of RNA synthesis, replication
857 mechanism, and in vitro RNA-dependent RNA polymerase activity of japanese
858 encephalitis virus. *Virology* **307**: 358-71. doi: 10.1016/s0042-6822(02)00130-7.
859 Villordo SM, Alvarez DE and Gamarnik AV. 2010. A balance between circular and linear
860 forms of the dengue virus genome is crucial for viral replication. *RNA* **16**: 2325-35. doi:
861 10.1261/rna.2120410.
862 Villordo SM, Carballada JM, Filomatori CV and Gamarnik AV. 2016. RNA Structure

863 Duplications and Flavivirus Host Adaptation. *Trends Microbiol.* doi:
864 10.1016/j.tim.2016.01.002.

865 Villordo SM, Filomatori CV, Sanchez-Vargas I, Blair CD and Gamarnik AV. 2015. Dengue
866 virus RNA structure specialization facilitates host adaptation. *PLoS Pathog* **11**: e1004604.
867 doi: 10.1371/journal.ppat.1004604.

868 Villordo SM and Gamarnik AV. 2009. Genome cyclization as strategy for flavivirus RNA
869 replication. *Virus Res* **139**: 230-9. doi: 10.1016/j.virusres.2008.07.016.

870 Vogt DA and Andino R. 2010. An RNA element at the 5'-end of the poliovirus genome
871 functions as a general promoter for RNA synthesis. *PLoS Pathog* **6**: e1000936. doi:
872 10.1371/journal.ppat.1000936.

873 Wang L, Jeng KS and Lai MM. 2011. Poly(C)-binding protein 2 interacts with sequences
874 required for viral replication in the hepatitis C virus (HCV) 5' untranslated region and
875 directs HCV RNA replication through circularizing the viral genome. *J Virol* **85**: 7954-64.
876 doi: 10.1128/JVI.00339-11.

877 Wells SE, Hillner PE, Vale RD and Sachs AB. 1998. Circularization of mRNA by eukaryotic
878 translation initiation factors. *Mol Cell* **2**: 135-40.

879 Welsch S, Miller S, Romero-Brey I, Merz A, Bleck CK, Walther P, Fuller SD, Antony C,
880 Krijnse-Locker J and Bartenschlager R. 2009. Composition and three-dimensional
881 architecture of the dengue virus replication and assembly sites. *Cell Host Microbe* **5**:
882 365-75. doi: 10.1016/j.chom.2009.03.007.

883 Wu B, Grigull J, Ore MO, Morin S and White KA. 2013. Global organization of a
884 positive-strand RNA virus genome. *PLoS Pathog* **9**: e1003363. doi:

885 10.1371/journal.ppat.1003363.

886 Wu B, Pogany J, Na H, Nicholson BL, Nagy PD and White KA. 2009. A discontinuous

887 RNA platform mediates RNA virus replication: building an integrated model for RNA-based

888 regulation of viral processes. *PLoS Pathog* **5**: e1000323. doi:

889 10.1371/journal.ppat.1000323.

890 Yap TL, Xu T, Chen YL, Malet H, Egloff MP, Canard B, Vasudevan SG and Lescar J. 2007.

891 Crystal structure of the dengue virus RNA-dependent RNA polymerase catalytic domain at

892 1.85-angstrom resolution. *J Virol* **81**: 4753-65. doi: 10.1128/JVI.02283-06.

893 Yoffe AM, Prinsen P, Gelbart WM and Ben-Shaul A. 2011. The ends of a large RNA

894 molecule are necessarily close. *Nucleic Acids Res* **39**: 292-9. doi: 10.1093/nar/gkq642.

895 You S and Padmanabhan R. 1999. A novel in vitro replication system for Dengue virus.

896 Initiation of RNA synthesis at the 3'-end of exogenous viral RNA templates requires 5'- and

897 3'-terminal complementary sequence motifs of the viral RNA. *J Biol Chem* **274**: 33714-22.

898 Zhang B, Dong H, Stein DA, Iversen PL and Shi PY. 2008. West Nile virus genome

899 cyclization and RNA replication require two pairs of long-distance RNA interactions.

900 *Virology* **373**: 1-13. doi: 10.1016/j.virol.2008.01.016.

901 Zhou Y, Ray D, Zhao Y, Dong H, Ren S, Li Z, Guo Y, Bernard KA, Shi PY and Li H. 2007.

902 Structure and function of flavivirus NS5 methyltransferase. *J Virol* **81**: 3891-903. doi:

903 10.1128/JVI.02704-06.

904 Zuker M. 2003. Mfold web server for nucleic acid folding and hybridization prediction.

905 *Nucleic Acids Res* **31**: 3406-15.

906 Zuker M and Jacobson AB. 1998. Using reliability information to annotate RNA secondary

907 structures. *RNA* **4**: 669-79.

908 **Figure legends**

909 **Figure 1.** Identification and comparison of the 5' UAR-UFS elements among flaviviruses.

910 **(A)** Terminal RNA structures of the DENV4 genome. The UAR, DAR and CS elements are

911 highlighted in yellow, green and red, respectively. Pseudoknotted interactions are labeled.

912 The UFS stem region is indicated by parentheses. **(B)** Comparison of the 5' UAR-UFS and

913 UFS-like elements in MBFVs, NKVs and ISFVs. *: KEDV and ZIKV were supposed to

914 belong to the same clade herein. The MBFV 5' UAR sequences and NKV sequences

915 involved in genome cyclization are colored in yellow. The nucleotides that participate in

916 the DAR interactions of MBFVs are labeled in green. Translational start codons in (A) and

917 (B) are shown in red. Virus name abbreviations are annotated in *Figure 1 - figure*

918 *supplement 2*.

919 The following figure supplements are available for figure 1:

920 **Figure supplement 1.** Circular conformation of the DENV4 genomic RNA.

921 **Figure supplement 2.** Molecular phylogenetic analysis of the flavivirus genus.

922 **Figure 2.** SHAPE analysis of the 5' end RNA of representative flaviviruses.

923 The SHAPE reactivity results are labeled in the structure models of different

924 flaviviruses. Highly reactive nucleotides (SHAPE reactivity > 0.85) are labeled in red,

925 whereas nucleotides with moderate SHAPE reactivity (0.4-0.85) are labeled in green.

926 Black-colored nucleotides indicate low or no SHAPE reactivity (< 0.4). Nucleotides

927 lacking SHAPE data are labeled in gray. The primer-binding region in the reverse

928 transcription reaction is shown in light blue. **(A)** JEV, strain SA-14-14-2 (AF315119). **(B)**

929 DENV1; the sequence is based on strain WestPac (U88535). (C) DENV2; the
930 sequence is based on strain NGC (KM204118). (D) DENV3; the sequence is based on
931 strain 80-2 (AF317645). (E) DENV4; strain 814669 (AF326573), with two artificial
932 nonsense mutations that do not affect the 5' end secondary structures or vRNA
933 replication. The two mutations, located in the loop region of cHP and DCS-PK Loop 3,
934 respectively, are labeled in black-colored font. (F) ZIKV; strain FSS13025 (KU955593).
935 Results presented were from two biological replicates.

936 The following source data and figure supplement are available for figure 2:

937 **Source data 1.** Source data for figure 2.

938 **Figure supplement 1.** SHAPE analysis of the DENV3 UFS mutants.

939 **Figure 3.** The secondary structure of the UFS is required for flavivirus vRNA
940 replication.

941 (A) The organization of the DENV4 replicon constructs. In
942 p4-cHPstop-SP-IRES-Rluc-Rep, the translation of viral nonstructural proteins is
943 controlled by the EMCV IRES, and artificial stop codons (red inverted triangles) were
944 introduced into the cHP loop region as well as the end of the capsid-coding region to
945 abolish translation directed by the 5' cap structure. In the improved version,
946 p4-Dualstop-SP-IRES-Rluc-Rep, one additional stop codon was introduced into loop 3
947 of the DCS-PK element to abolish the potential translational start from a cryptic AUG in
948 the 5' CS element. (B) Replication characteristics of the above two replicons in BHK-21
949 cells. Relative luciferase units are defined as the ratio of luciferase units measured at
950 different time points after transfection to the value measured at 6 h post-transfection.

951 (C) Demonstration of DENV4 UFS mutants. Mutations are shown in purple. The “A”
952 mutants contain mutations in the downstream strand of the UFS, and the “B” mutants
953 contain mutations in the upstream strand of the UFS. The “C” mutant in each group
954 combines the “A” and “B” mutations to restore the secondary structure of the UFS.
955 Note that the secondary structures shown here are for illustration only and do not
956 represent the actual folding of these mutants. (D) Replication efficiency of the UFS
957 mutants. The results of one of two independent biological replicates were shown. One
958 hundred nanograms per well of replicon RNA species were transfected into BHK-21
959 cells in triplicate. The results are expressed as the percentage of the relative luciferase
960 units of a UFS mutant at 72 h post-transfection to the value of the WT replicon (relative
961 replication efficiency). The error bar represents the standard deviation in all figures.
962 The mean values of relative replication efficiency are listed below the names of the
963 replicon constructs.

964 The following source data and figure supplement are available for figure 3:

965 **Source data 1.** Source data for figure 3 and figure 3-figure supplement 1.

966 **Figure supplement 1.** Replication of DENV4 UFS mutants targeting the AUG region .

967 **Figure 4.** SHAPE analysis of the DENV4 UFS mutants.

968 SHAPE analysis was performed for DENV4 5'-300 nt RNA containing the UFS
969 mutations M1A, M1C, M3A or M3C. The SHAPE result for WT 5' end RNA is shown in
970 parallel. SHAPE diagrams of 5' 20-200 nt are shown, and the regions corresponding to
971 various 5' elements are indicated. Negative SHAPE reactivity is set to zero. The
972 SHAPE reactivity of the 5' UAR-UFS region is annotated on the corresponding

973 secondary structures (left). Nucleotides with SHAPE reactivity greater than 0.85 are
974 labeled in red, and moderately reactive sites (0.4-0.85) are labeled in green. Unlabeled
975 sites have low or no SHAPE reactivity (< 0.4). Two biological replicates were performed
976 for each RNA , and the error bars represent the standard deviation.

977 The following source data is available for figure 4:

978 **Source data 1.** Source data for figure 4.

979 **Figure 5.** The role of the UFS in viral propagation.

980 **(A)** DENV4 UFS M5 series mutants. Mutations are shown in purple. **(B-D)** vRNA
981 replication profiles of different UFS mutants in transfected BHK-21 cells. WT and
982 NS5-inactive GVD mutant vRNA, measured in parallel, are shown as controls. **(B)** M1
983 series, **(C)** M3 series and **(D)** M5 series. **(E)** Indirect immunofluorescence assay of WT,
984 GVD, and UFS-mutated vRNA-transfected BHK-21 cells. **(F)** Determination of the virus
985 titers in the supernatants of the M1 series mutant-transfected BHK-21 cells. The virus
986 titers in the supernatants of WT vRNA-transfected cells were determined in parallel.
987 The virus titers were normalized according to input vRNA copies determined at 4 h
988 post-electroporation. **(G-I)** The RNA stability of the UFS mutants was determined by
989 qRT-PCR and are expressed as the fold change relative to the vRNA copies at 4 h
990 post-transfection. **(G)** M1 series, **(H)** M3 series and **(I)** M5 series. Results were from
991 one biological replicate. Experiments to determine vRNA copies and virus titers were
992 performed in triplicate. Note that the time point “72 h” for the GVD group in **(D)** contains
993 data from only two parallel wells (technical replicates), because the result of the third
994 sample was unreliable due to an error in RNA isolation process.

995 The following source data and figure supplement are available for figure 5:

996 **Source data 1.** Source data for 5B and 5C.

997 **Source data 2.** Source data for 5D.

998 **Source data 3.** Source data for 5F.

999 **Source data 4.** Source data for 5G, 5H and 5I.

1000 **Figure supplement 1.** Replication of ZIKV UFS mutants in BHK-21 cells.

1001 **Figure 6.** UFS is crucial for RdRp recruitment and *de novo* RNA synthesis.

1002 **(A)** Simplified diagrams of DENV4 virus 5' end RNA constructs used for RdRp binding
1003 and/or *in vitro* RdRp activity assays. The region corresponding to the UFS element is
1004 shown in blue, and the red regions represent the genome cyclization elements. **(B)**
1005 SDS-PAGE of purified recombinant NS5Pol of DENV4. **(C)** The binding of DENV4
1006 NS5Pol to 5'-300 nt RNA molecules containing UFS mutations was analyzed by EMSA.
1007 No NS5Pol was present in the left first lane of each group. The NS5Pol concentrations
1008 in the reactions were approximately 2.0, 3.5, 5.0 and 7.5 μ M (from left to right). **(D)** *In*
1009 *vitro* RdRp activity assay using 5'-160 nt RNA as a template. The reactions were
1010 incubated at 30 °C for 20 min. Detection was based on the incorporation of
1011 biotin-11-CTP into the products. Left, the results of the M1 series; right, the results of
1012 the M3 series. Two bands were detectable in the blot: the upper template-sized band
1013 was generated by the terminal addition of biotin-11-CTP to the input template due to
1014 the terminal nucleotide transferase activity of NS5Pol in the presence of Mn^{2+} , and the
1015 lower band represented the dsRNA product of *de novo* RNA synthesis, which was
1016 confirmed by comparison of the electrophoretic patterns of the RdRp products and

annealed dsRNA molecules (*Figure 6-figure supplement 2*). **(E)** EMSA was performed for the 5'-160 nt RNA molecules containing M1 series mutations. The NS5Pol concentrations in the reactions were approximately 3.6, 7.2, 10.7 and 14.3 μ M (left to right).

The following figure supplements are available for figure 6:

Figure supplement 1. The UFS is required for efficient NS5 binding to 5' RNA in JEV.

Figure supplement 2. Identification of the products of the RdRp reactions.

Figure 7. Effect of UFS stability on vRNA replication.

(A) Demonstration of UFS mutants. The mutations are indicated in purple. The M2C mutant contained two UA-to-GC base pair substitutions, whereas the M4C mutant contained four substitutions in the UFS secondary structure. It should be noted that the secondary structures are meant for illustration purposes only, and the structures displayed for UFS-disrupted mutants are not the most thermodynamically favorable ones. **(B)** Relative replication efficiency of UFS mutants shown in (A). The results of one of two independent biological replicates were shown. Fifty nanograms per well of replicon RNA were transfected into 96-well plates. Experiments were performed in triplicate.

The following source data and figure supplements are available for figure 7:

Source data 1. Source data for figure 7 and figure 7-figure supplement 1.

Figure supplement 1. Effects of mutations in the SLB-UFS internal loop on vRNA replication.

Figure supplement 2. NS5Pol binding assay of the DENV4 5'-300 nt M2A and M2C

1039 mutants.

1040 **Figure 8.** Increasing the stability of the UFS hinders vRNA cyclization.

1041 (A) Schematic diagram of experimental design. As 5'-300 nt RNA is incubated with 3'
1042 UTR RNA, a 5'-3' RNA bimolecular complex is formed due to the interactions that
1043 promote genome cyclization. Various RNA structural elements in the DENV4 genomic
1044 ends are shown. The regions involved in terminal interactions are colored in red, and
1045 the UFS element is labeled in blue. (B) RNA binding assay of the UFS mutants. 3' UTR
1046 RNA (20 ng/μl) was incubated with different amounts (16, 40, 80 and 160 ng/μl) of
1047 various 5'-300 nt RNA mutants in 20-μl reactions. The formation of RNA complexes
1048 was then analyzed by native TBE PAGE gels. A gel image of the M1 series mutants is
1049 shown on the top, and the results for the M2 series mutants are shown below. The
1050 molar ratios between 5' and 3' RNA are indicated above the gel lanes.

1051 The following figure supplements are available for figure 8:

1052 **Figure supplement 1.** RNA binding assay of the UFS L1D, L3D and M3 series
1053 mutants.

1054 **Figure supplement 2.** The calculation of binding affinity of 3' UTR for the 5'-300 nt
1055 RNAs.

1056 **Figure 9.** SHAPE analysis of the interactions between DENV4 genomic ends.

1057 (A) SHAPE analysis was performed for DENV4 5'-300 nt WT and M2C RNA in the
1058 presence of various amounts of 3' UTR RNA. For convenience, only the results for
1059 nucleotides 60-150, which include critical elements for genome cyclization, are shown.
1060 Regions corresponding to various 5' elements are indicated. Negative SHAPE

1061 reactivity is set to zero for clear demonstration.. **(B)** The changes in the SHAPE
1062 reactivity of the 5' 60-150 region were obtained by subtracting the SHAPE reactivity
1063 when 3' UTR RNA was absent from the corresponding values when 3' UTR RNA was
1064 present in a 1:1 ratio with 5'-300 nt RNA. Results were from two biological replicates,
1065 and the error bars represent the standard deviation.

1066 The following source data is available for figure 9:

1067 **Source data 1.** Source data for figure 9.

1068 **Figure 10.** Genome cyclization disables the function of the UFS in NS5 recruitment.

1069 **(A)** Schematic diagram showing the conformational changes of the DENV4 genome.

1070 Two major conformations of vRNA, the linear and circular form, exist in equilibrium.

1071 The regions involved in terminal interactions are colored in red, and the UFS element is

1072 labeled in blue. The locations and sequences of the Δ SLA, cHP-M and CS-M mutants

1073 used in this section are indicated. **(B)** The conformational equilibrium of mini-genome

1074 RNA containing different mutations was analyzed using native PAGE. The bands of the

1075 linear and circular conformations were identified using the CS-M mutant as a control.

1076 The faint and much larger bands were likely to be formed by misfolded RNA molecules.

1077 **(C)** The binding of NS5Pol to different mini-genome RNA molecules was analyzed by

1078 EMSA. Mini-genomes containing the M1 series mutations in the UFS were assayed,

1079 and the WT and CS-M mini-genomes served as control reactions. No NS5Pol was

1080 present in the left first lane of each group. The NS5Pol concentrations in the reactions

1081 were approximately 2.0, 3.5, 5.0 and 7.5 μ M (from left to right). **(D)** *In vitro* RdRp

1082 activity assay using various mini-genome RNA molecules as templates. The reactions

1083 were performed at 30 °C for 40 min. Note that the signal of the Δ SLA lane did not
1084 correspond to the dsRNA product generated by *de novo* initiation. The blot was
1085 scanned by ImageJ software and RdRp activity was expressed as percentage of WT.
1086 Note that the template activity of M1C-mini was calculated by scanning a longer
1087 exposed version of the same blot shown.

1088 **Figure 11.** Model explaining the functional mechanism of the UFS switch.

1089 A proposed mechanistic model of flavivirus vRNA replication. (i) After the viral genome
1090 is released into the cytoplasm, first, translation occurs on the circularized genome to
1091 generate a sufficient level of viral proteins for downstream vRNA synthesis. (ii)
1092 Accumulation of viral replication proteins (only NS5 and NS3 are shown) to high
1093 concentrations results in the formation of an RNA-viral replicase complex and initiates
1094 (-) RNA synthesis to generate the double-stranded replication form (RF). (iii) Then, the
1095 synthesis of nascent (+) RNA using RF as the template is initiated by NS5/viral
1096 replicase. During the process, 5' local structures including UFS are formed in the
1097 displaced, parental (+) strand RNA. A free NS5/viral replicase is recruited to bind the 5'
1098 end of the displaced (+) RNA. (iv) As soon as the nascent (+) strand RNA synthesis
1099 completes, the released (+) ssRNA genome is circularized by terminal interactions, and
1100 the next round of (-) strand synthesis is ready to start.

1101 **Figure 12.** Genome conformation models of major groups of flaviviruses.

1102 Sequences involved in terminal interactions are shown in red. The 5' RNA structures
1103 that are immediately downstream of SLA elements and consistently involved in
1104 genome cyclization are indicated by red arrows. The typical UFS element in MBFVs is

1105 shown in blue. The demonstrated structures are based on DENV4 for the MBFVs;
 1106 tick-borne encephalitis virus (TBEV) for TBFVs; Wesselsbron virus (WESSV) for the
 1107 YFV clade of the MBFVs and RBV for the NKVs. The kissing loop interaction identified
 1108 recently in the tick-borne group (*Tsetsarkin et al., 2016*) is labeled by green letters (KL).
 1109 The following figure supplements are available for figure 12:

1110 **Figure supplement 1.** Terminal genomic RNA structures of the MBFV group.

1111 **Figure supplement 2.** Terminal genomic RNA structures of the YFV clade in the
 1112 MBFV group.

1113 **Figure supplement 3.** Terminal genomic RNA structures of the TBFV group.

1114 **Figure supplement 4.** Terminal genomic RNA structures of the NKV group.

1115 **Titles and legends for figure supplements**

1116 **Figure 1 - figure supplement 1.** Circular conformation of the DENV4 genomic RNA.
 1117 The UAR, DAR and CS elements are shown in yellow, green and red, respectively. The
 1118 sequence of the unwound UFS duplex is shown in blue.

1119 **Figure 1 - figure supplement 2.** Molecular phylogenetic analysis of the flavivirus genus.
 1120 The ORF sequences of 48 flavivirus species were obtained from Genbank and aligned by
 1121 Clustal W method. The evolutionary relationships of flaviviruses were inferred by using the
 1122 Maximum Likelihood method based on the Tamura-Nei model. Analyses were performed
 1123 with MEGA6. Different evolutionary groups as well as various clades among the MBFV
 1124 group are annotated.

1125 **Figure 2 - figure supplement 1.** SHAPE analysis of the DENV3 UFS mutants.
 1126 SHAPE analysis of DENV3 5'-300 nt RNA molecules containing UFS mutations. the

SHAPE result of WT 5'-300 nt RNA is shown in parallel. SHAPE diagrams of 5' 20-250 nt are shown, and the regions corresponding to various 5' elements are indicated. Negative SHAPE reactivity is set to zero. The SHAPE reactivity of the 5' UAR-UFS region is annotated on the corresponding secondary structures. Nucleotides with SHAPE reactivity greater than 0.85 are labeled in red, moderately reactive sites (0.4-0.85) are labeled in green. Unlabeled sites have low or no SHAPE reactivity (< 0.4). Two biological replicates were performed for each RNA .

Figure 3 – figure supplement 1. Replication of DENV4 UFS mutants targeting the AUG region.

(A) Demonstration of mutants targeting the AUG start codon. Mutation sites are shown in purple. These mutants were designed without affecting either genome cyclization or the terminal topology of circularized genome. For detailed information, please refer to supplementary file 3. (B) Relative replication efficiency of UFS mutants shown above at 48 h post transfection. Results shown were obtained from three parallel technical replicates.

Figure 5 - figure supplement 1. Replication of ZIKV UFS mutants in BHK-21 cells.

Indirect immunofluorescence assay of WT and UFS-mutated ZIKV vRNA-transfected BHK-21 cells were performed. The secondary structures of mutants were demonstrated and mutation sites are shown in purple.

Figure 6 - figure supplement 1. The UFS is required for efficient NS5 binding to 5' RNA in JEV.

The binding of JEV NS5Pol to 5'-320 nt RNA molecules containing UFS mutations was analyzed by EMSA. No NS5Pol was present in the left first lane of each group. The

1149 NS5Pol concentrations in the reactions were approximately 3.3, 5.0, 6.6 and 7.5 μ M
 1150 (from left to right).

1151 **Figure 6 - figure supplement 2.** Identification of the products of the RdRp reactions.

1152 Lane 1: dsRNA prepared by the annealing of the positive and negative strand of DENV4
 1153 5'-160 nt RNA. Lane 2-4: products of RdRp assays using different 5'-160 nt RNAs as
 1154 templates. Lane 2: WT, Lane 3: M2A, Lane 4: M2C.

1155 **Figure 7 - figure supplement 1.** Effects of mutations in the SLB-UFS internal loop on
 1156 vRNA replication.

1157 **(A)** Demonstration of mutants targeting the internal loop between SLB and UFS. Mutation
 1158 sites are shown in purple. **(B)** Relative replication efficiency of UFS mutants shown above.

1159 Results shown were obtained from two parallel technical replicates.

1160 **Figure 7 - figure supplement 2.** NS5Pol binding assay of the DENV4 5'-300 nt M2A and
 1161 M2C mutants.

1162 The binding of NS5Pol to 5'-300 nt WT, M2A and M2C RNA was analyzed by EMSA assay.
 1163 The left first lane in each group contained no NS5Pol. The NS5Pol concentrations in the
 1164 reactions were approximately 2.0, 3.5, 5.0 and 7.5 μ M (from left to right).

1165 **Figure 8 - figure supplement 1.** RNA binding assay of the UFS L1D, L3D and M3 series
 1166 mutants.

1167 3' UTR RNA (20 ng/ μ l) was incubated with different amount (16, 40, 80 and 160 ng/ μ l) of
 1168 the corresponding 5'-300 nt RNA mutants in 20- μ l reactions. The formation of RNA
 1169 complexes was then analyzed by native TBE PAGE gels. The molar ratios between 5' and
 1170 3' RNA are indicated above the gel lanes.

1171 **Figure 8 - figure supplement 2.** The calculation of binding affinity of 3' UTR for the
1172 5'-300 nt RNAs.

1173 Reactions containing a series of concentrations of different 5'-300 nt RNAs and fixed
1174 concentration (approximately 36.9 nM) of 3' UTR RNA were resolved in native PAGE gels.
1175 The gels were analyzed by ImageJ software and the percentages of bound 3' UTR RNA
1176 were calculated. We assumed that the band intensity has a positive linear correlation with
1177 the molecular weights of the corresponding molecules, and that was taken in account in
1178 the calculation. The plotted data was fitted with $\%Bound = [X]/(K_d + [X])$ using GraphPad
1179 Prism 6 (GraphPad Software, La Jolla, California, USA), where %Bound is the percentage
1180 of bound 3' UTR RNA, and [X] is the concentration of 5'-300 nt RNA. By this method, the
1181 K_d was estimated and showed along with the binding curve.

1182 **Figure 12 - figure supplement 1.** Terminal genomic RNA structures of the MBFV group.
1183 The demonstrated sequence was based on DENV4. Sequences involved in genome
1184 cyclization are highlighted in yellow. The gray regions are not included in the
1185 demonstration of Figure 12. The *mfold* software and *VARNA* application were utilized to
1186 generate the structural models.

1187 **Figure 12 - figure supplement 2.** Terminal genomic RNA structures of the YFV clade in
1188 the MBFV group.

1189 The demonstrated sequence was based on WESSV. Sequences involved in genome
1190 cyclization are highlighted in yellow. The gray regions are not included in the
1191 demonstration of Figure 12. The *mfold* software and *VARNA* application were utilized to
1192 generate the structural models.

1193 **Figure 12 - figure supplement 3.** Terminal genomic RNA structures of the TBFV group.

1194 The demonstrated sequence was based on TBEV. Sequences involved in genome
1195 cyclization are highlighted in yellow. The gray regions are not included in the
1196 demonstration of Figure 12. The *mfold* software and *VARNA* application were utilized to
1197 generate the structural models.

1198 **Figure 12 - figure supplement 4.** Terminal genomic RNA structures of the NKV group.

1199 The demonstrated sequence was based on RBV. Sequences involved in genome
1200 cyclization are highlighted in yellow. The gray regions are not included in the
1201 demonstration of Figure 12. The *mfold* software and *VARNA* application were utilized to
1202 generate the structural models.

1203 **List of source data and supplementary files**

1204 **Figure 2 - source data 1.** Source data for figure 2.

1205 **Figure 3 - source data 1.** Source data for 3B, 3D and figure 3 - figure supplement 1.

1206 **Figure 4 - source data 1.** Source data for figure 4.

1207 **Figure 5 - source data 1.** Source data for 5B and 5C.

1208 **Figure 5 - source data 2.** Source data for 5D

1209 **Figure 5 - source data 3.** Source data for 5F

1210 **Figure 5 - source data 4.** Source data for 5G, 5H and 5I.

1211 **Figure 7 - source data 1.** Source data for figure 7 and figure 7 - figure supplement 1.

1212 **Figure 9 - source data 1.** Source data for figure 9.

1213 **Supplementary file 1.** *Mfold* prediction for the terminal RNA structures of different
1214 flaviviruses.

1215 **Supplementary file 2.** *Mfold* prediction for the 5' end RNA structures of yokose virus

1216 clade of NKV group.

1217 **Supplementary file 3.** *Mfold* prediction for analysis of the influence of DENV4 UFS

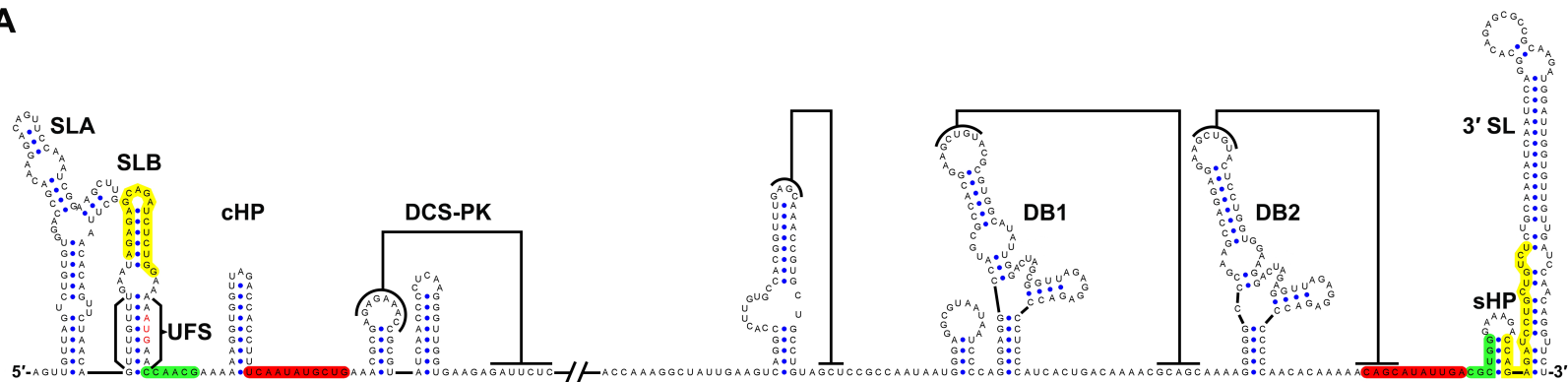
1218 mutations on the overall genome terminal RNA structures.

1219 **Supplementary file 4.** Structure models of DENV4 5' WT, M1A, M1C, M3A and M3C RNA

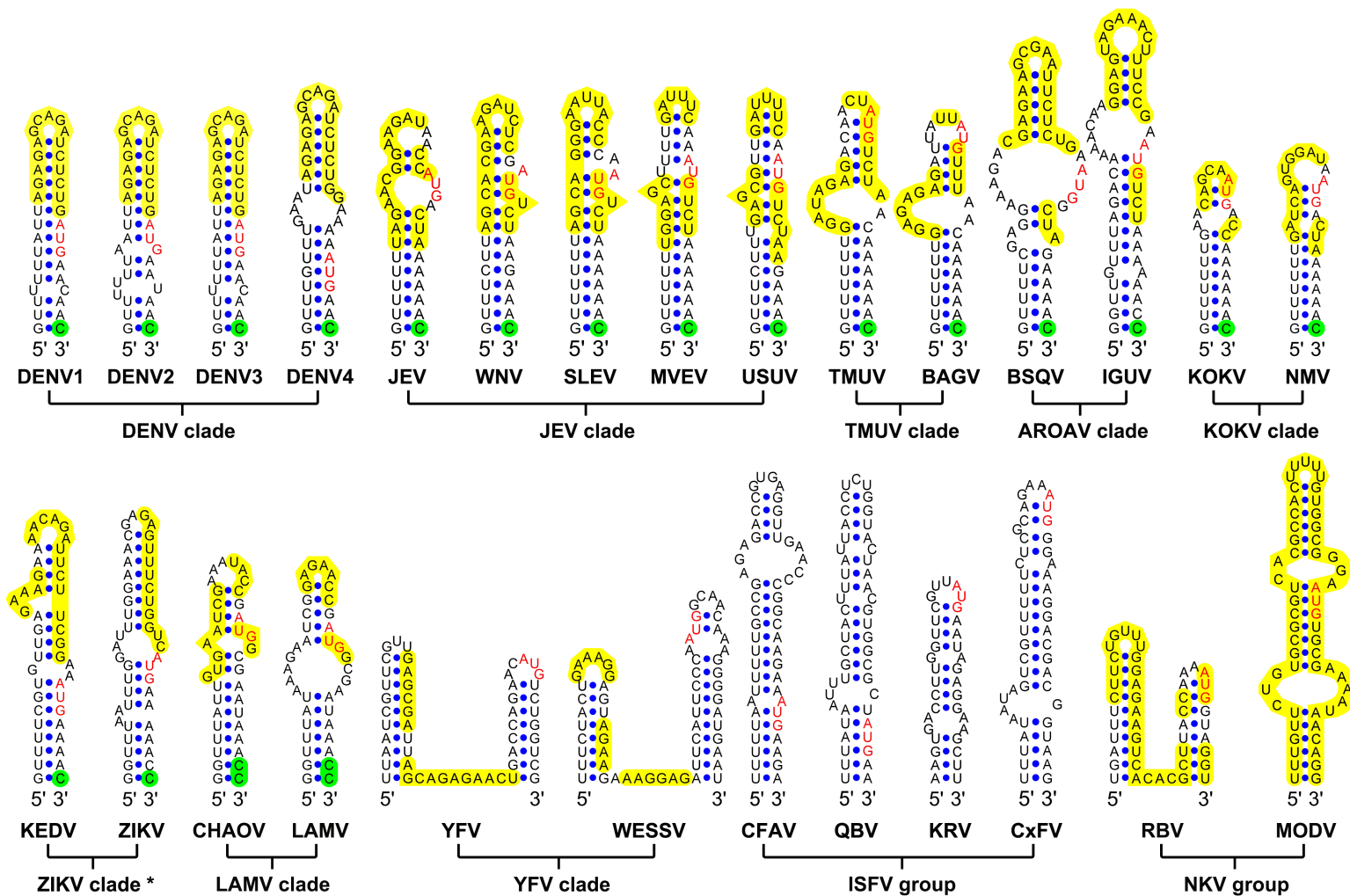
1220 generated by *RNAstructure* software using SHAPE constraints.

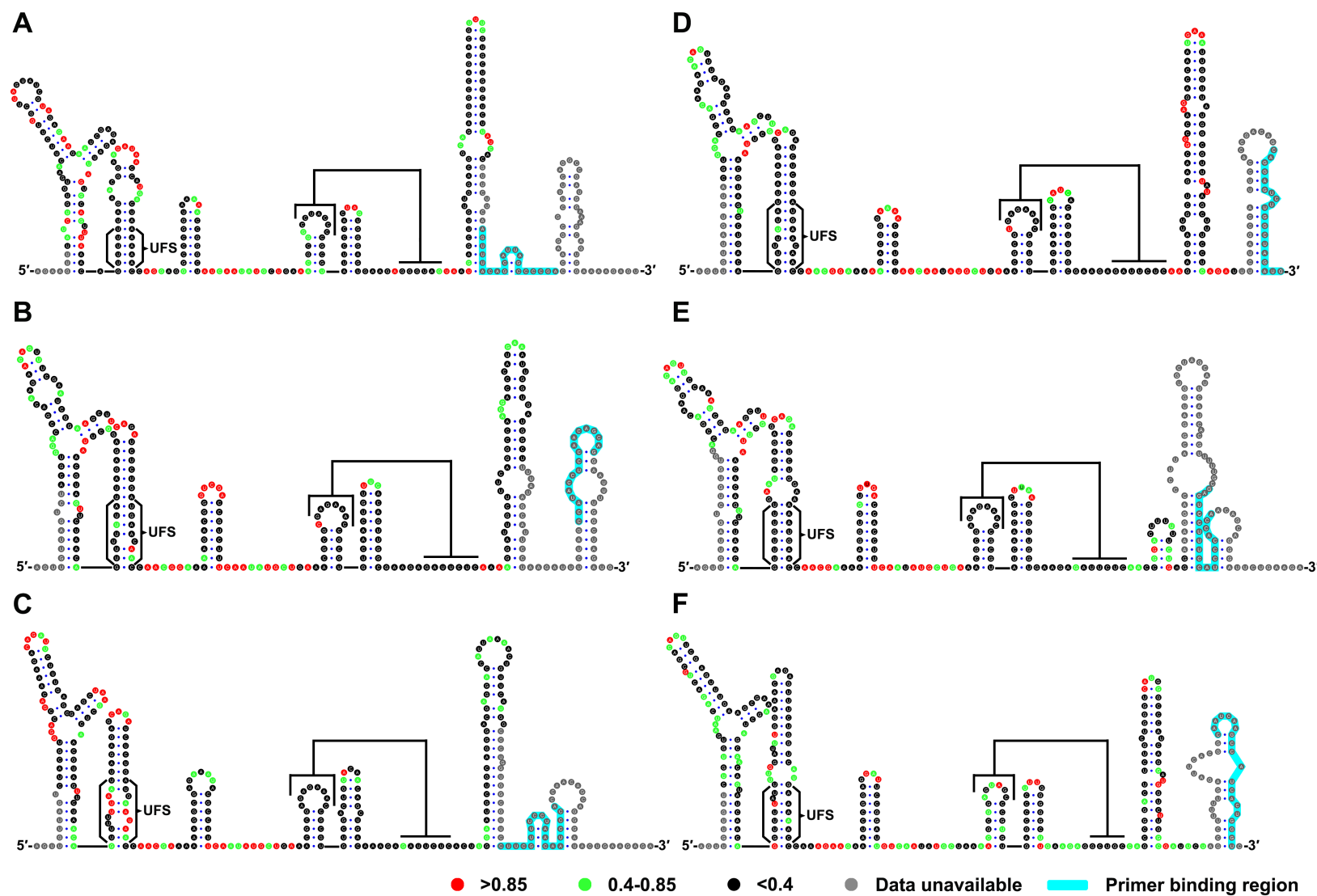
1221

A

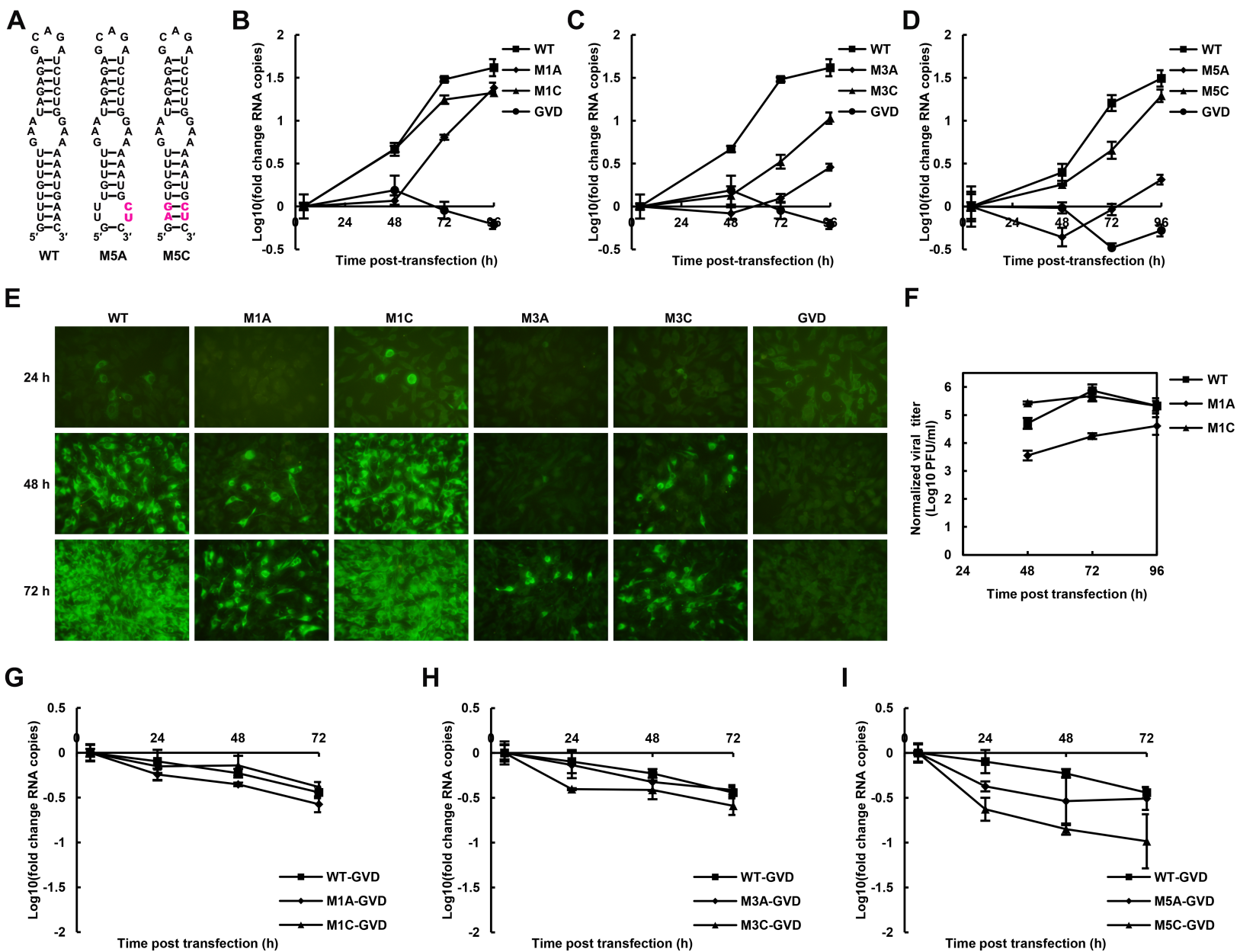


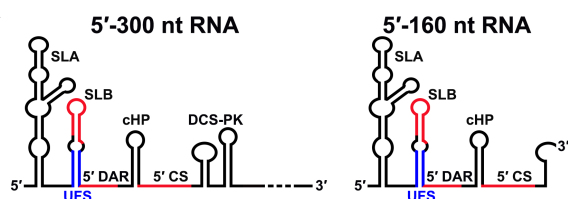
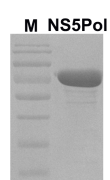
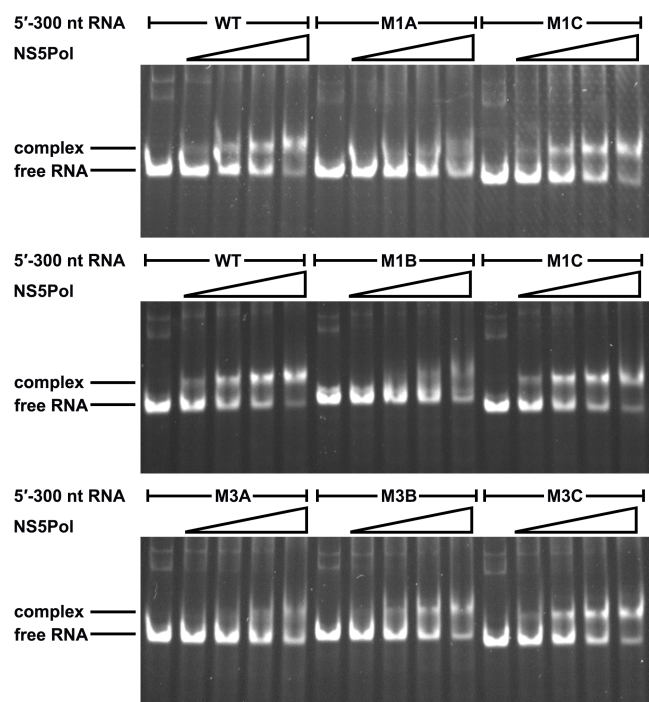
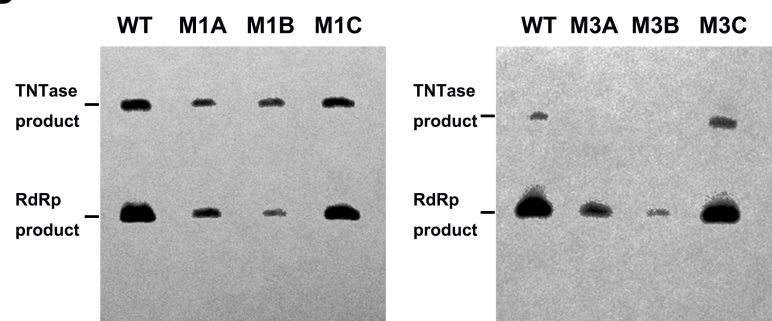
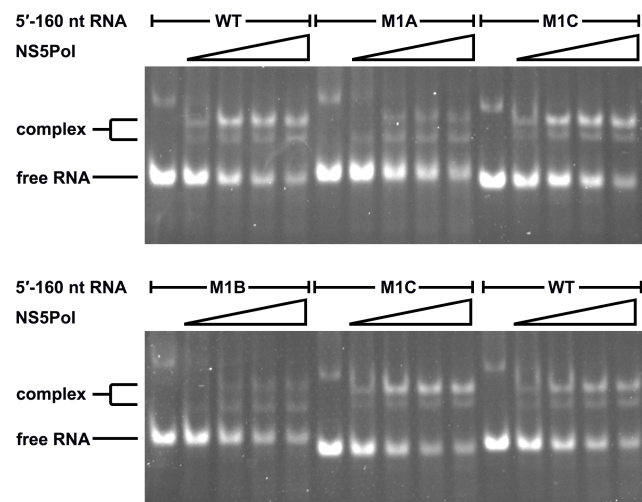
B



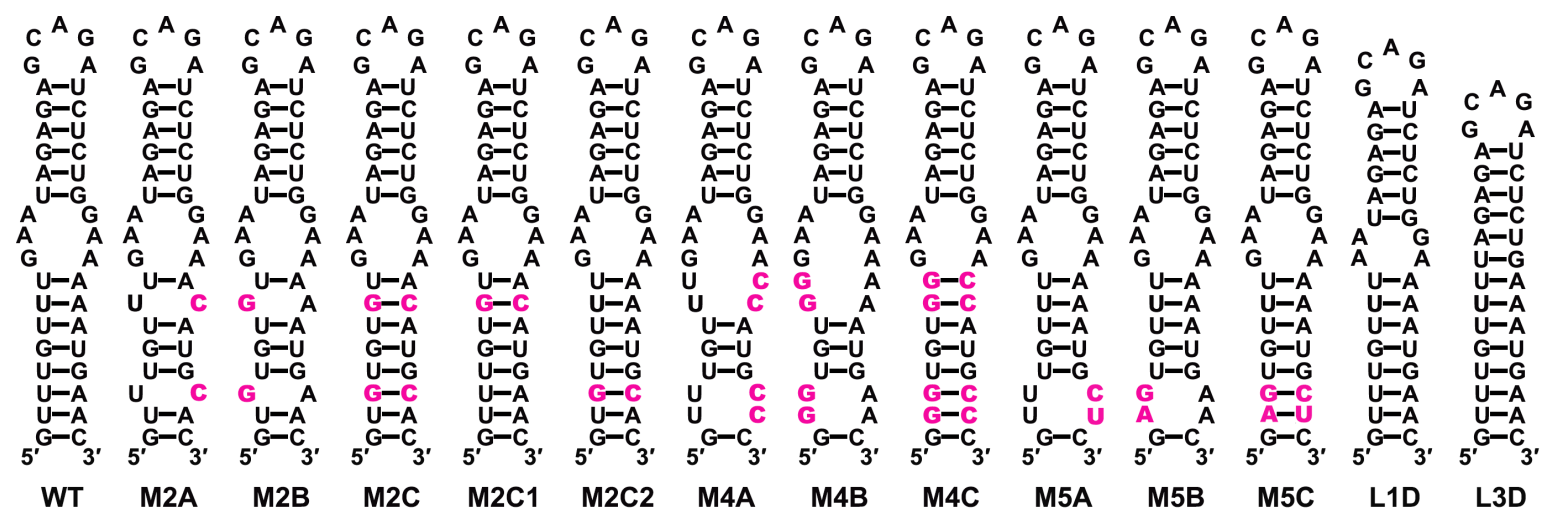




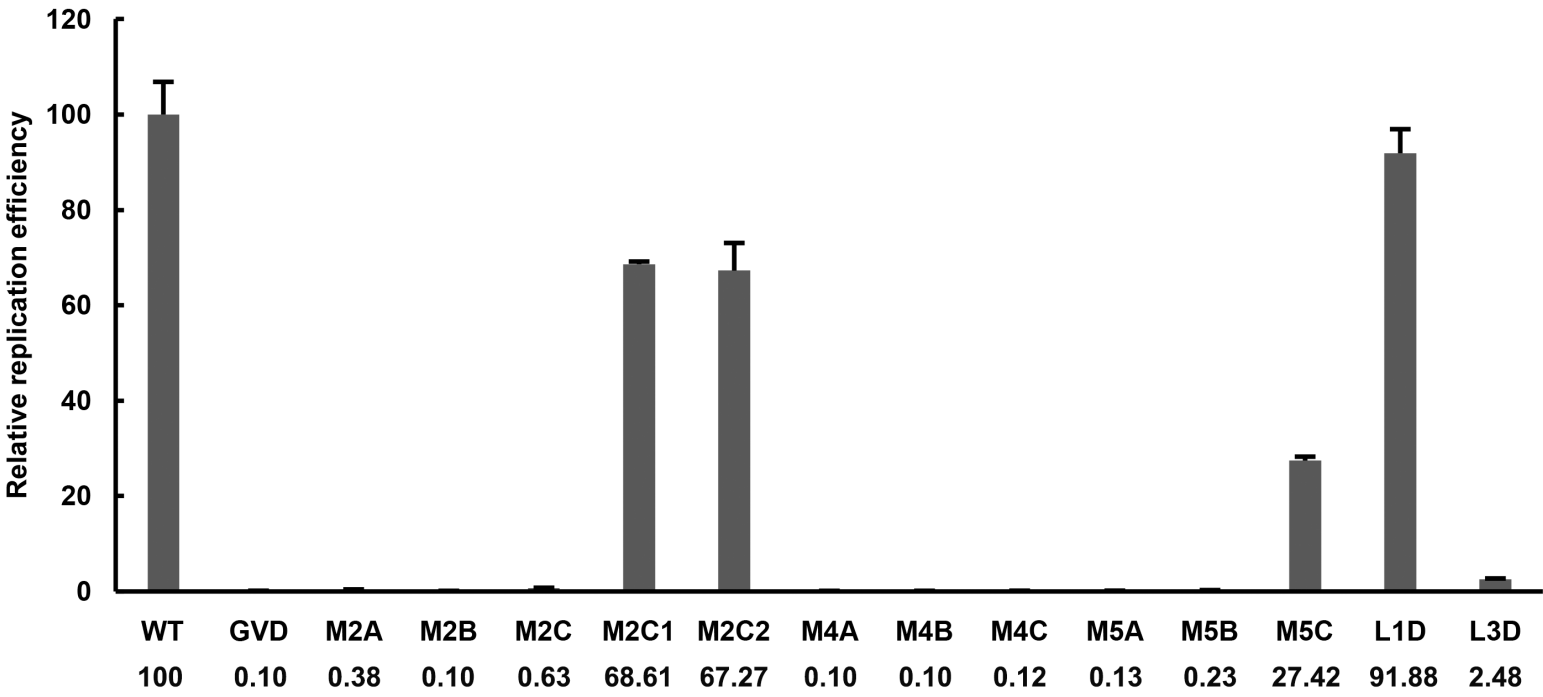


A**B****C****D****E**

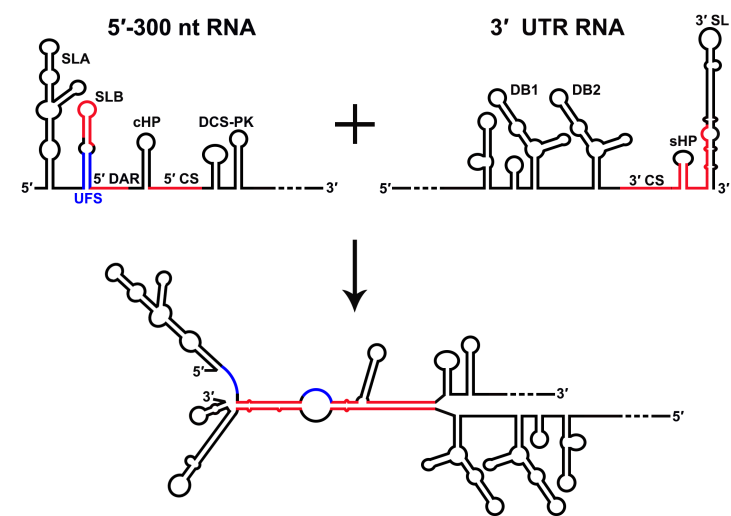
A



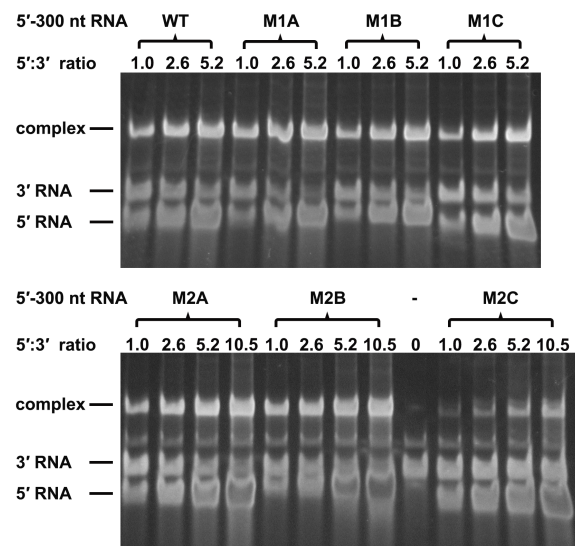
B



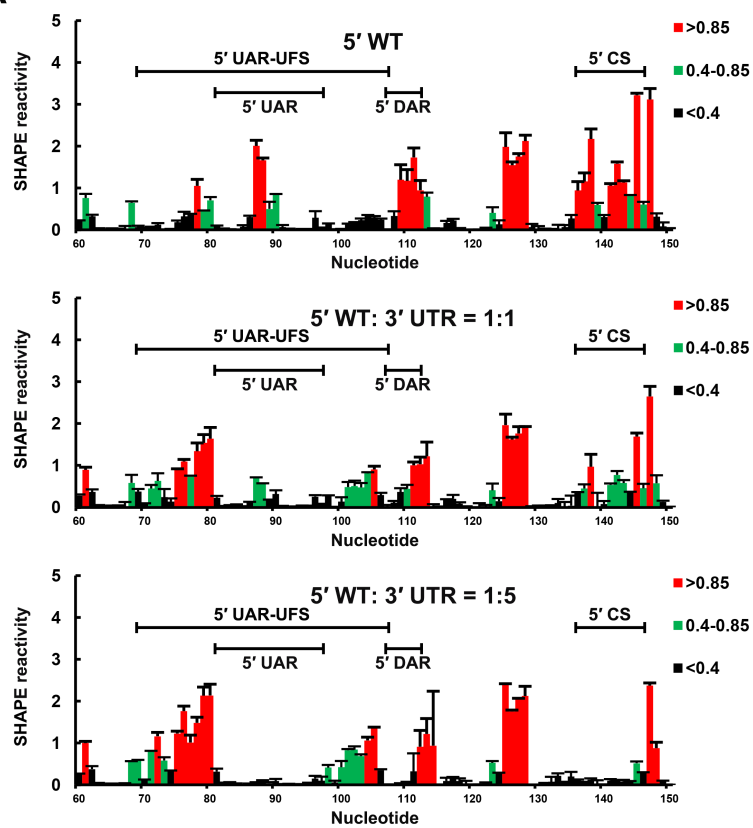
A



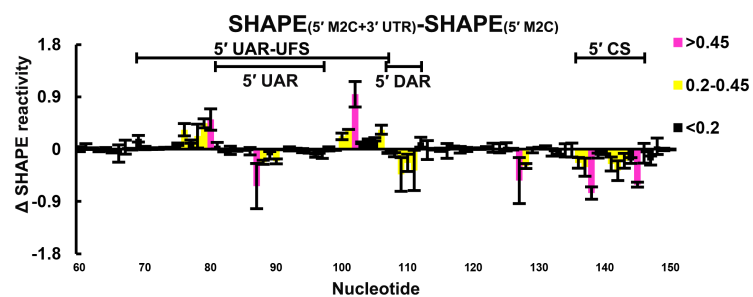
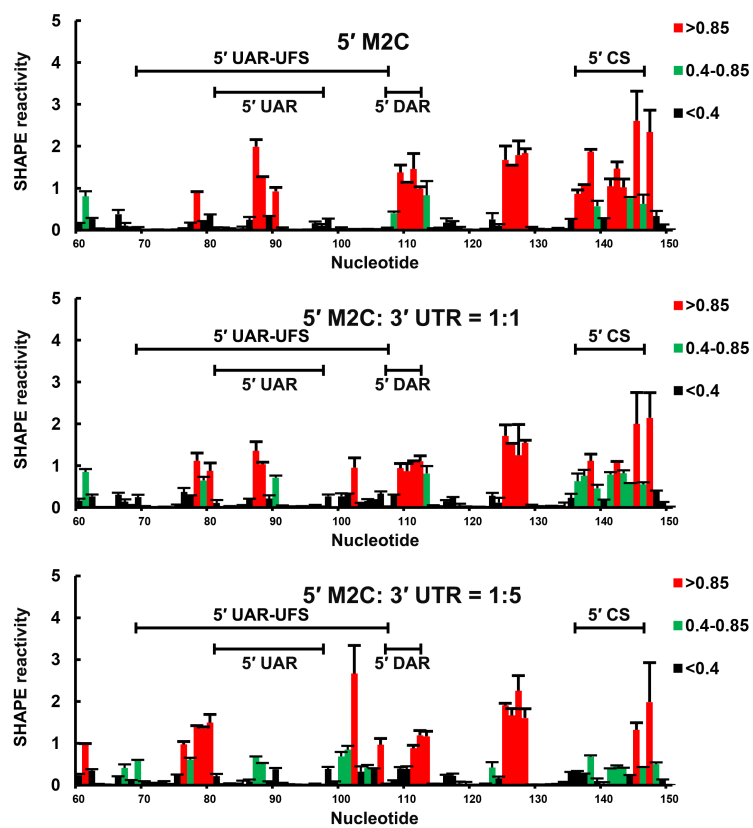
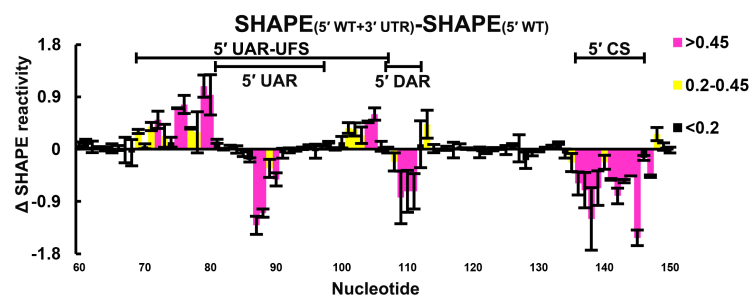
B

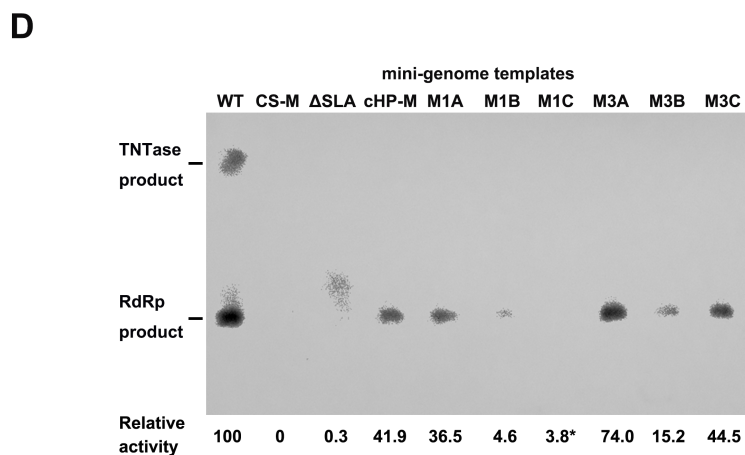
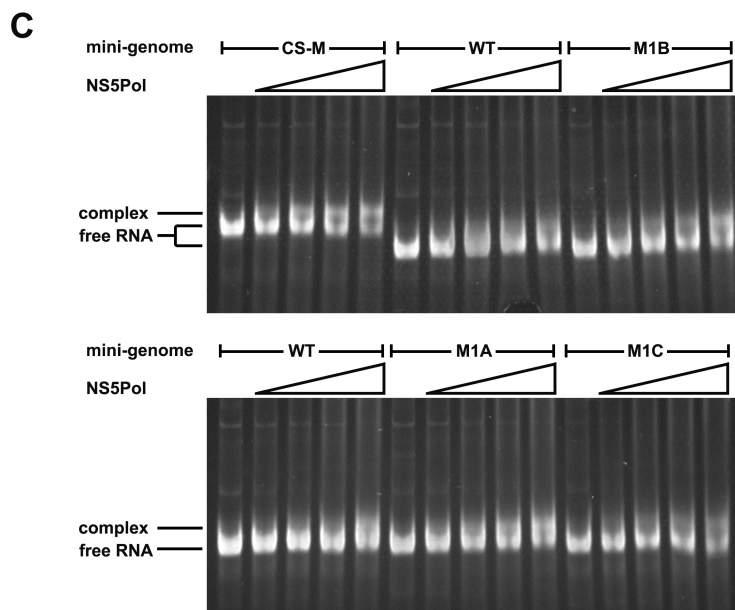
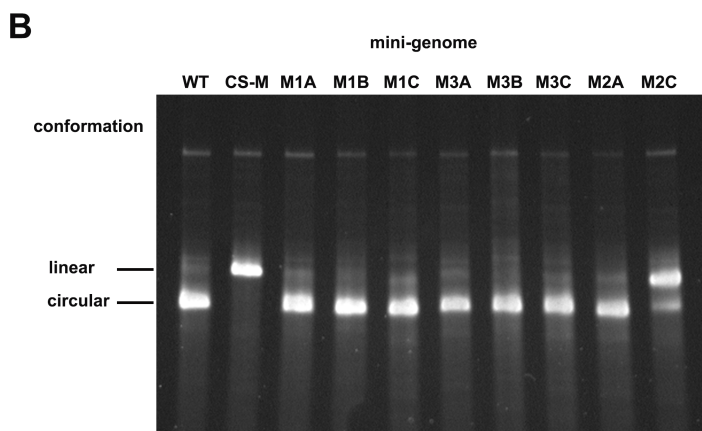
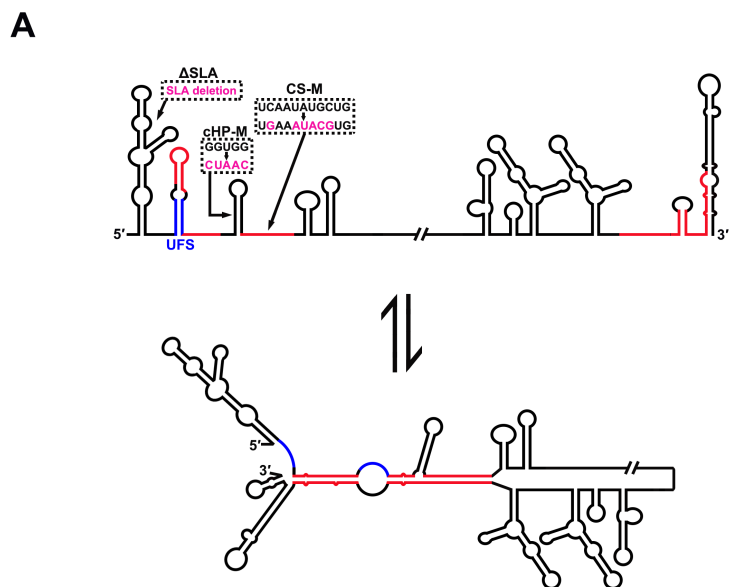


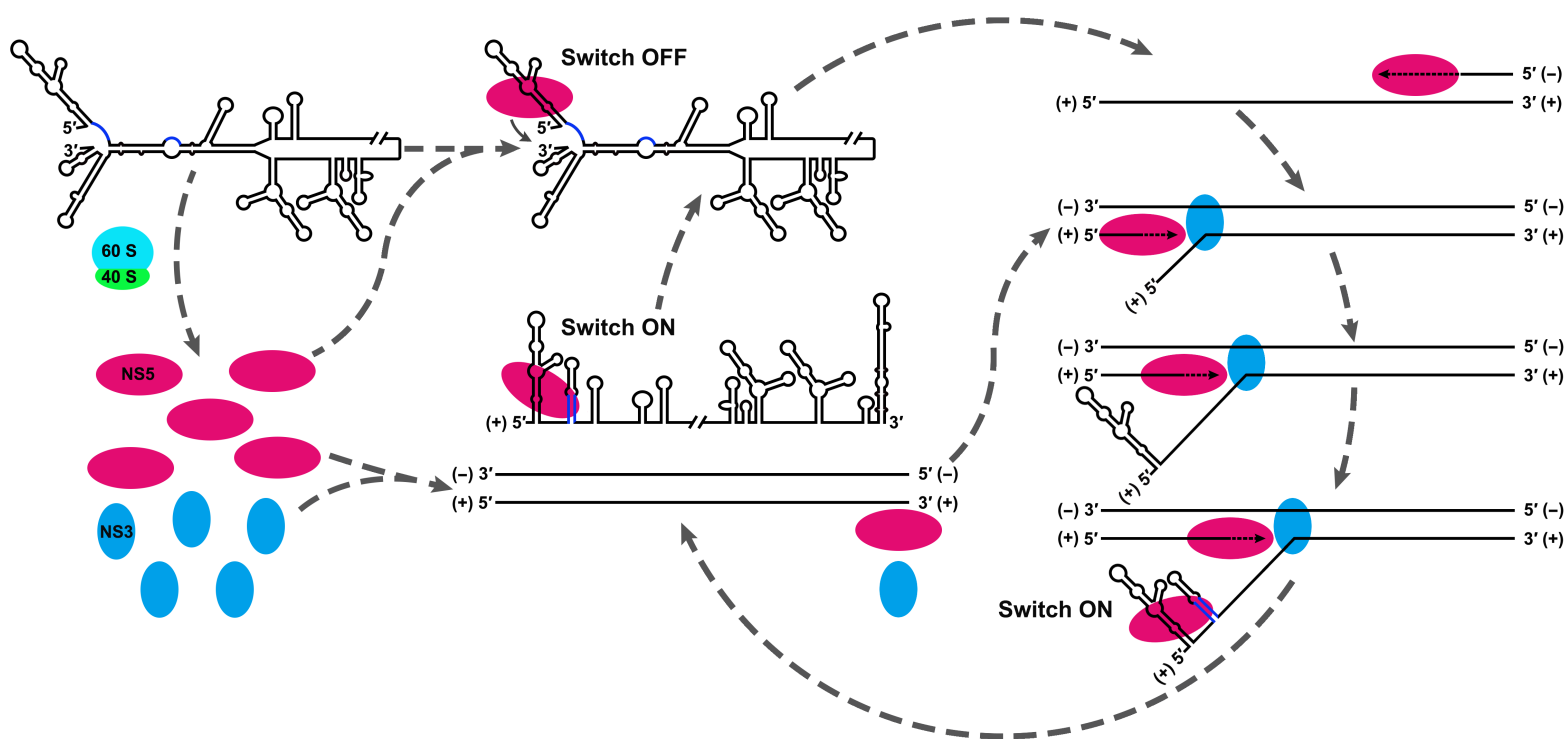
A

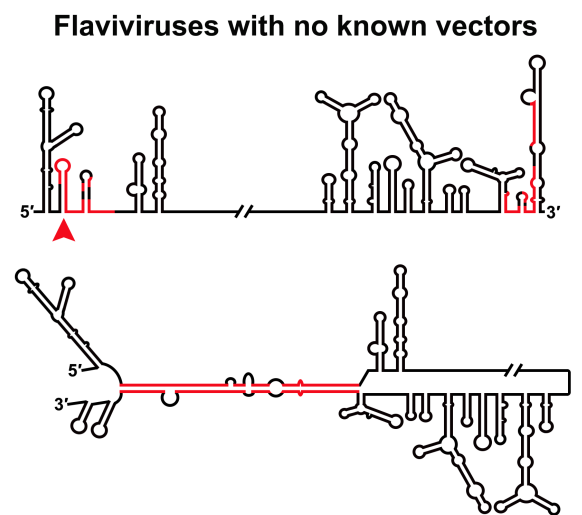
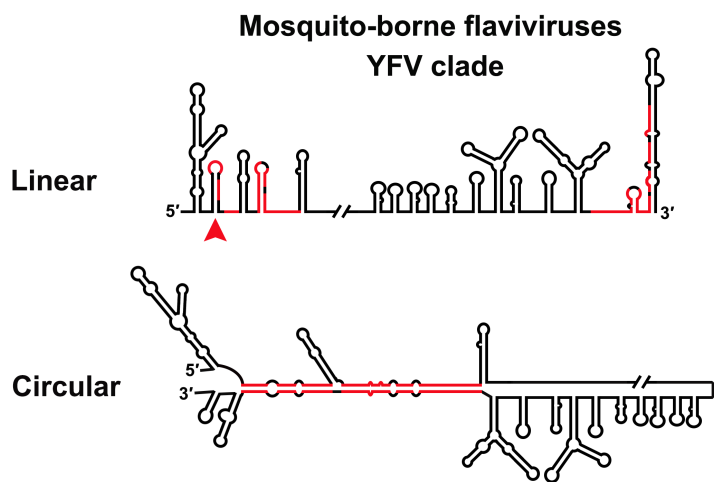
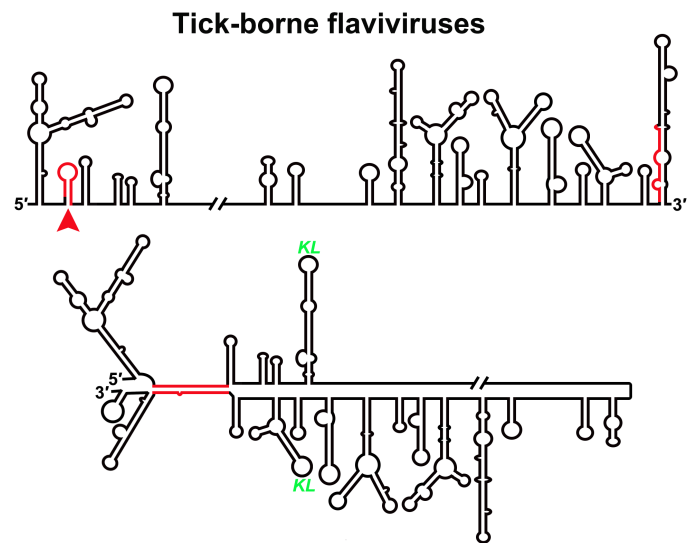
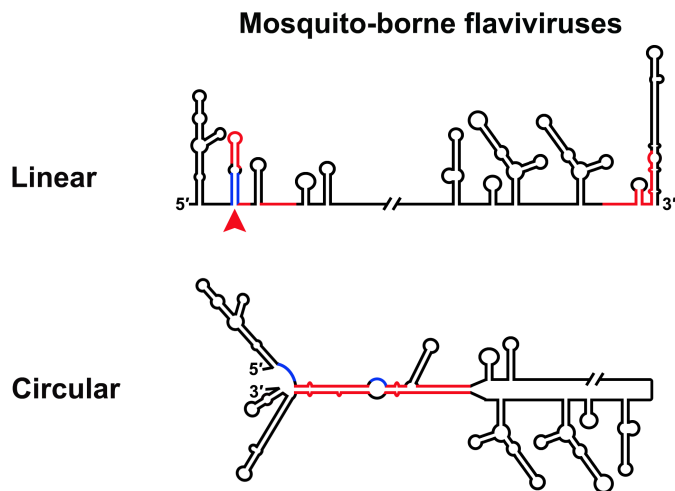


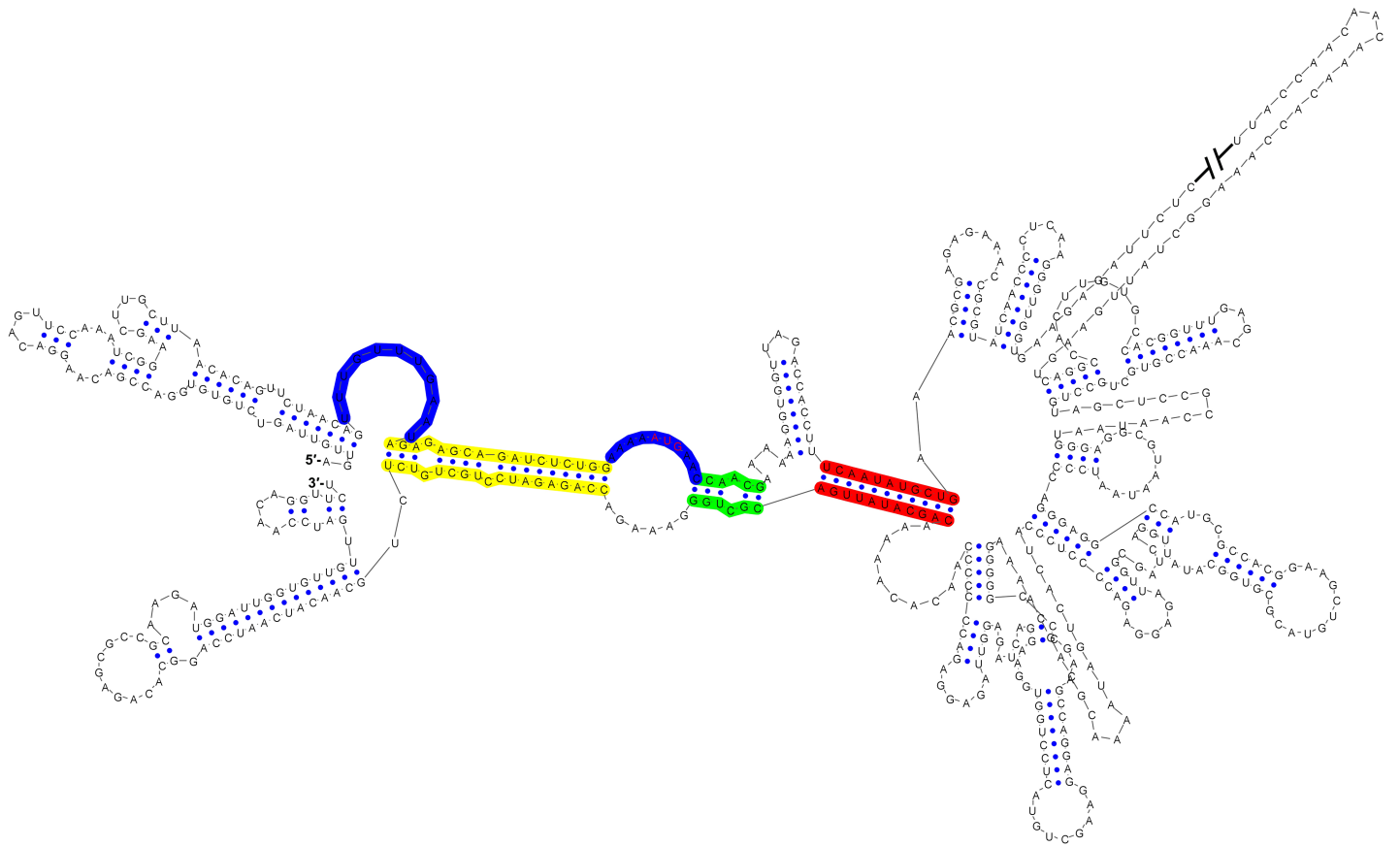
B

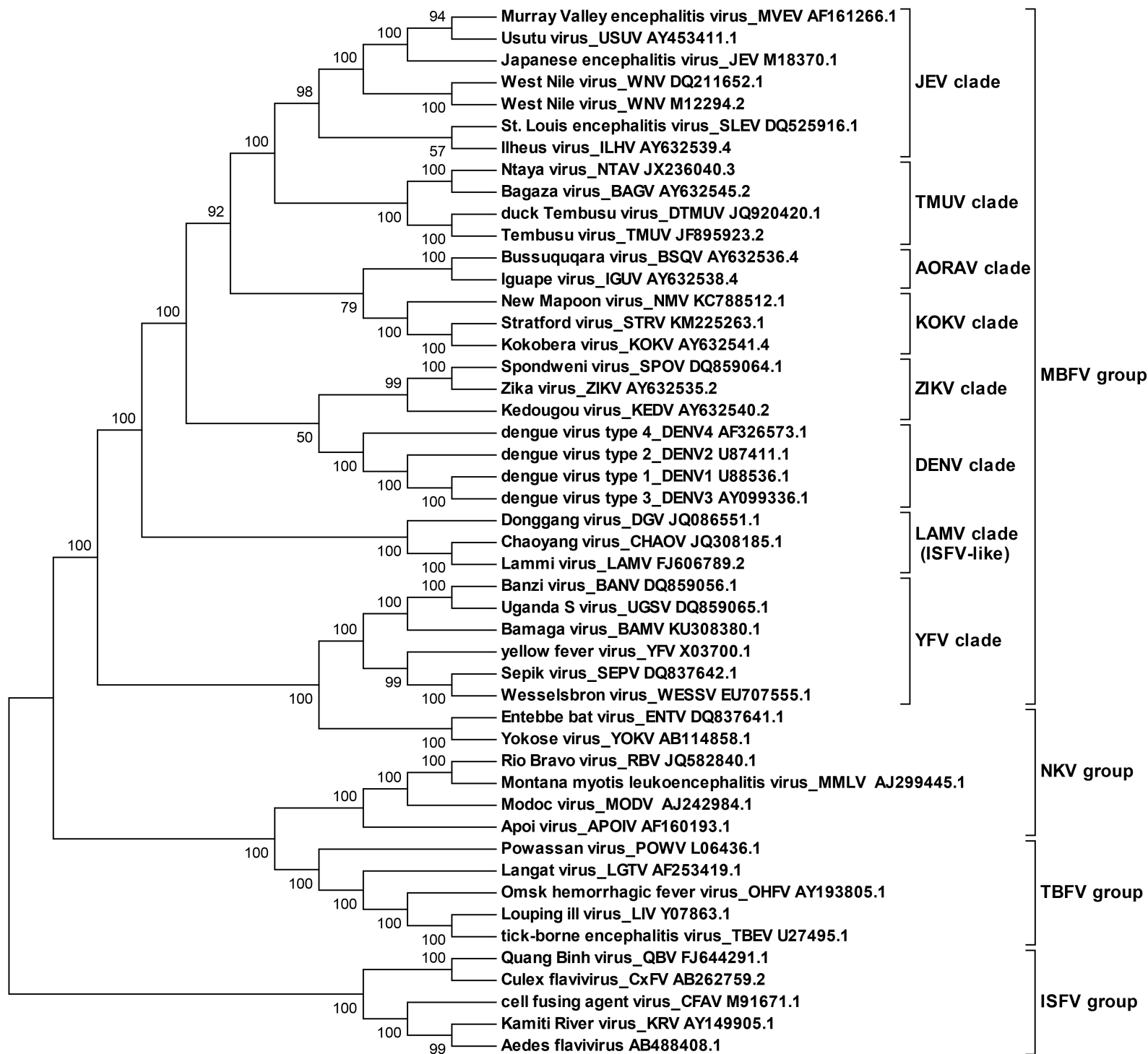






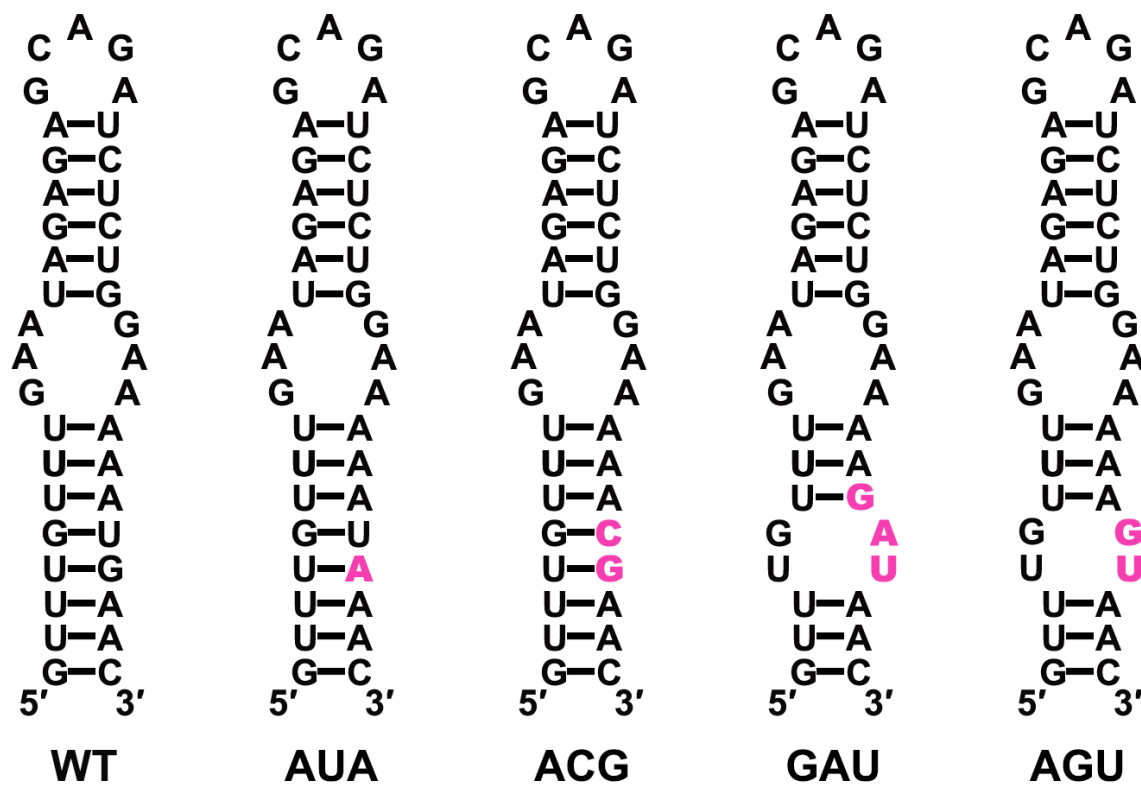




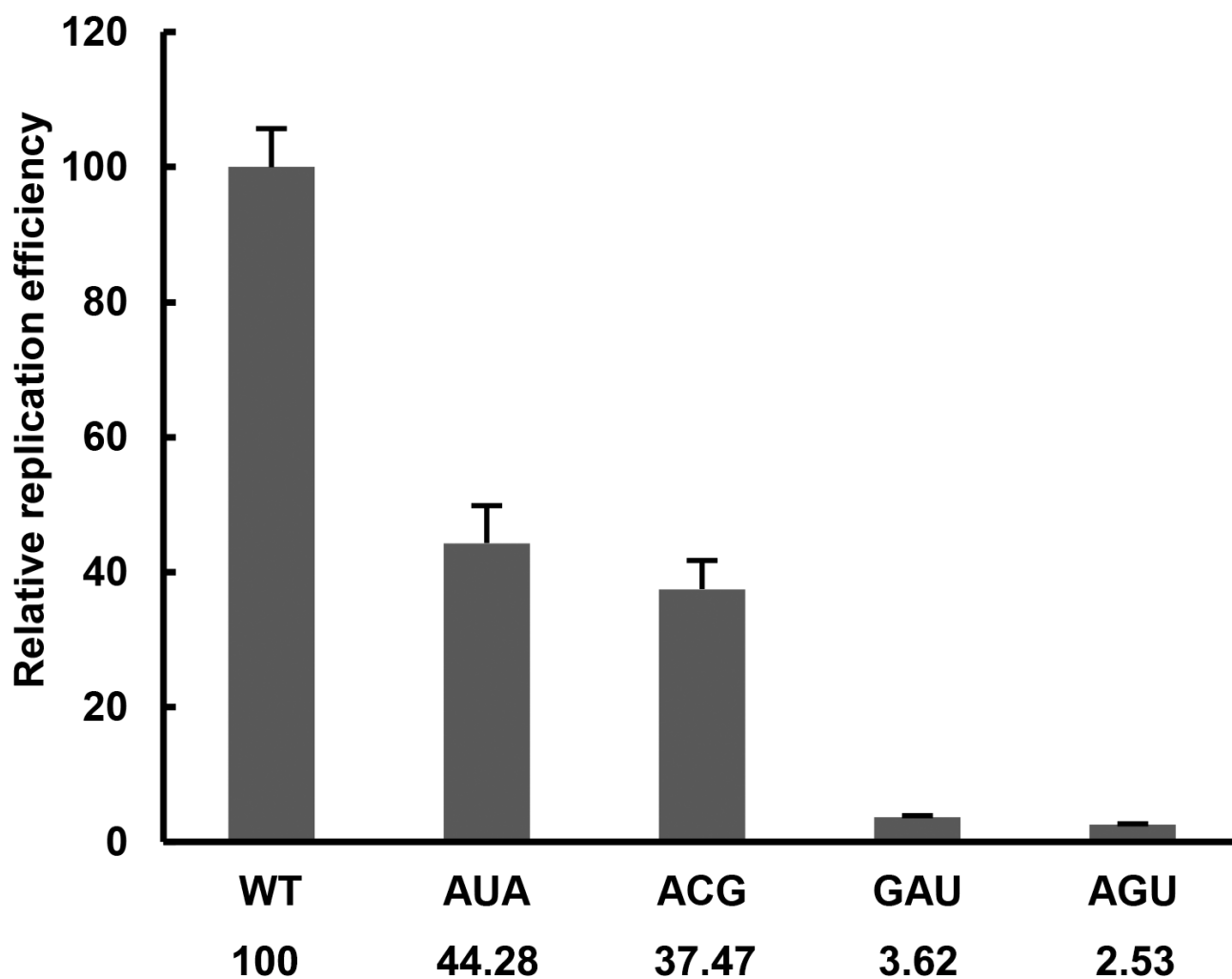


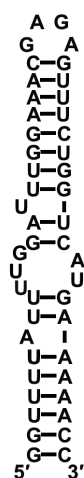


A

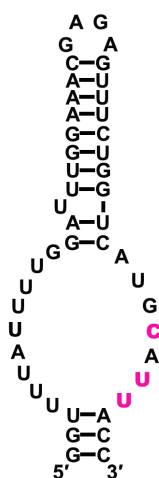


B

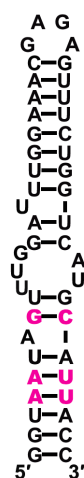




ZIKV-WT

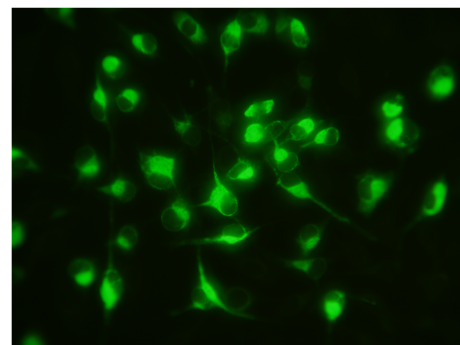
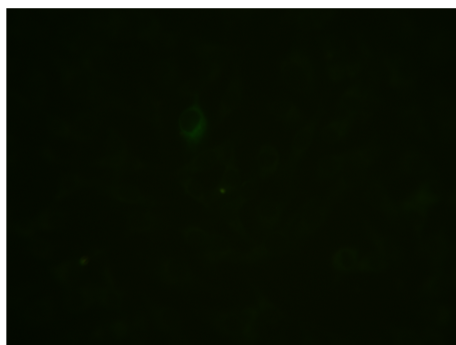
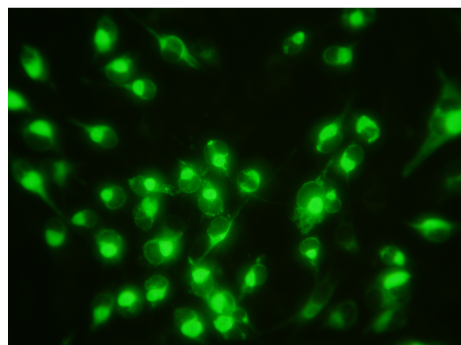


ZIKV-M3A

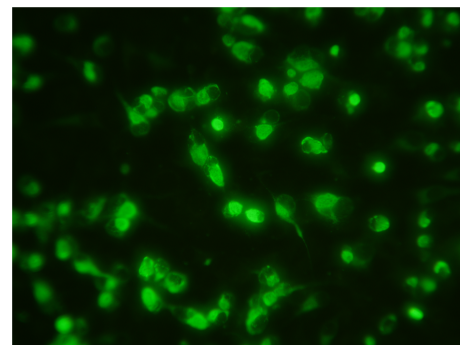
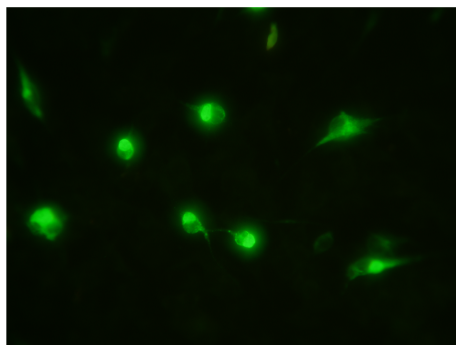
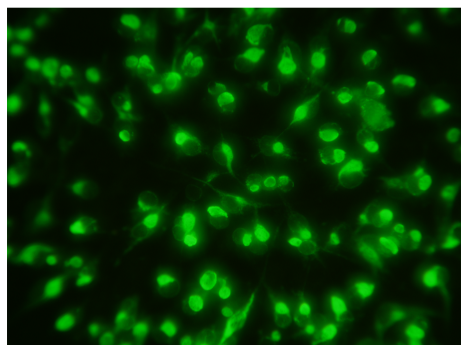


ZIKV-M3C

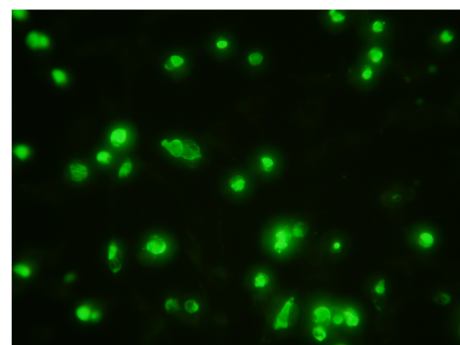
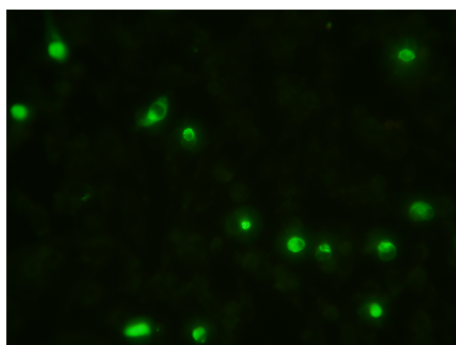
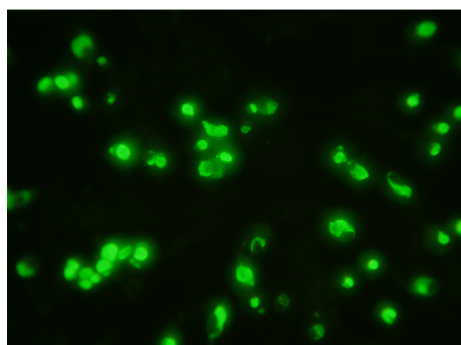
24 h



48 h



72 h



[illegible]

5'-320 nt RNA
JEV-NS5Pol

JEV-M1A

JEV-M1C

complex —
free RNA —

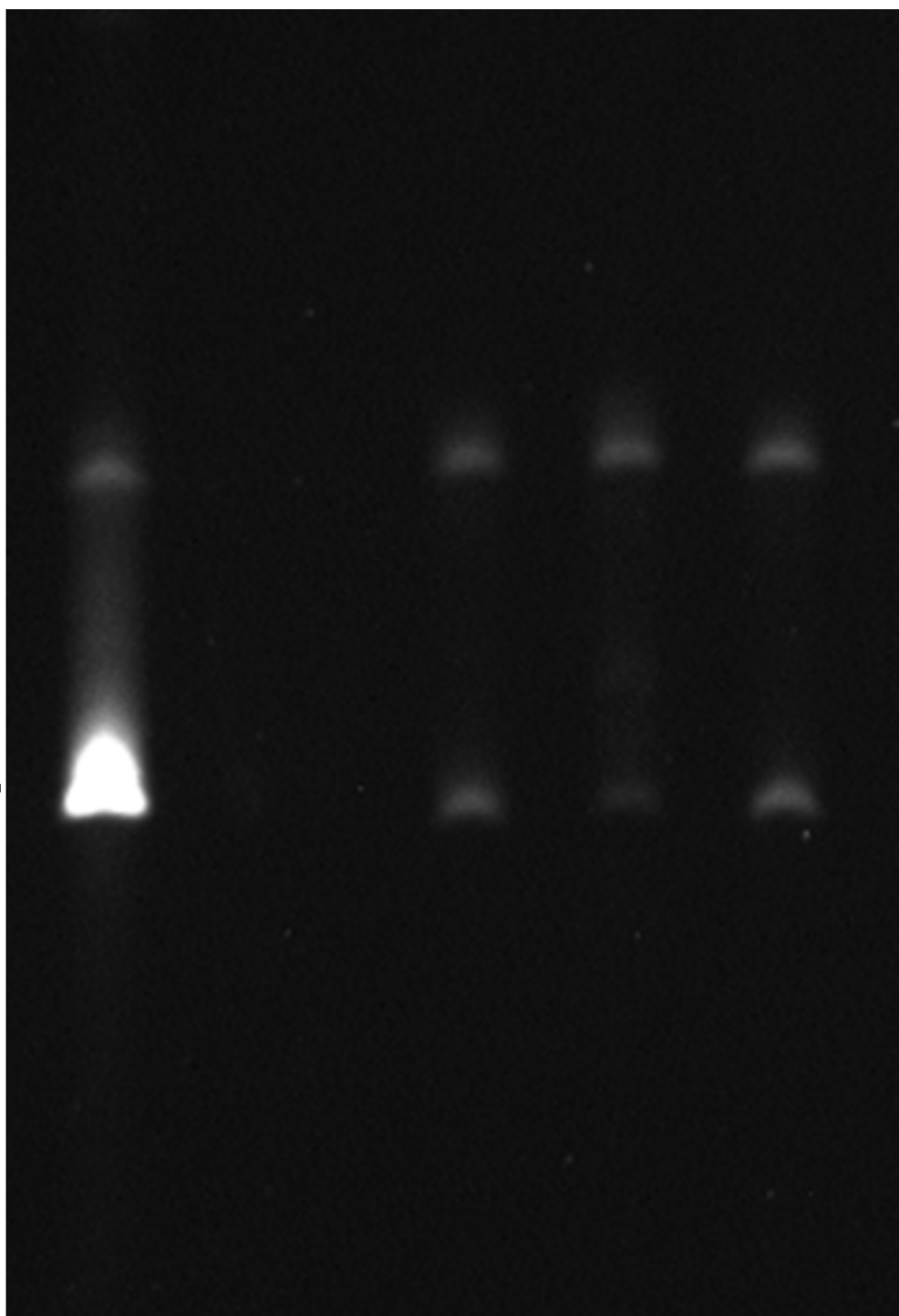
1

2

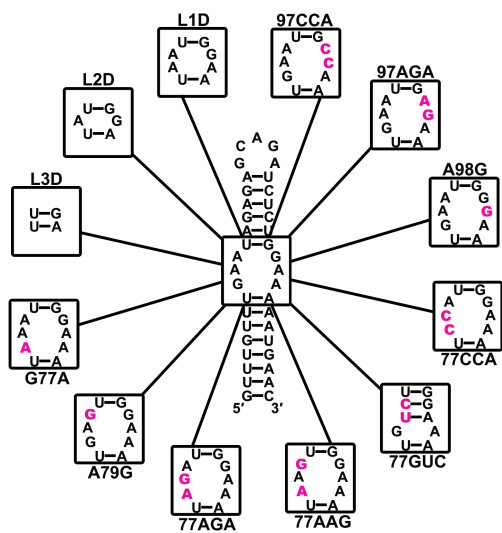
3

4

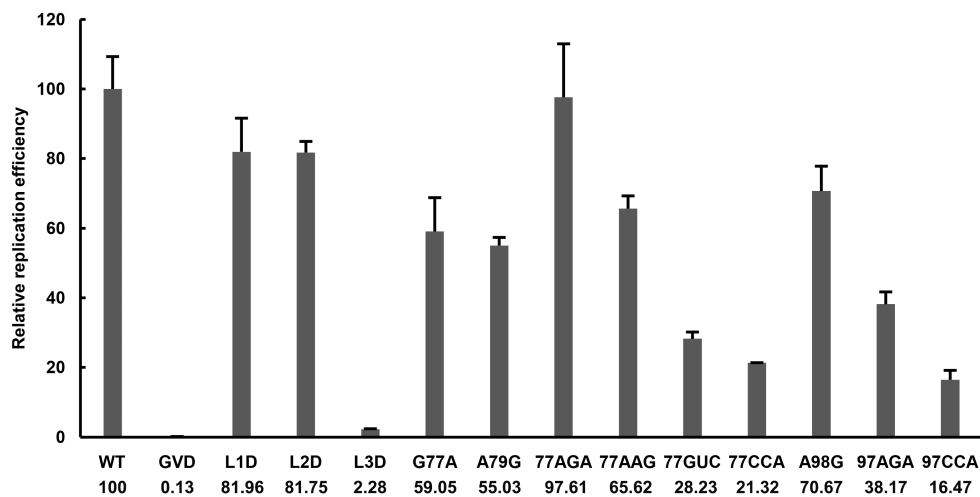
dsRNA—



A



B



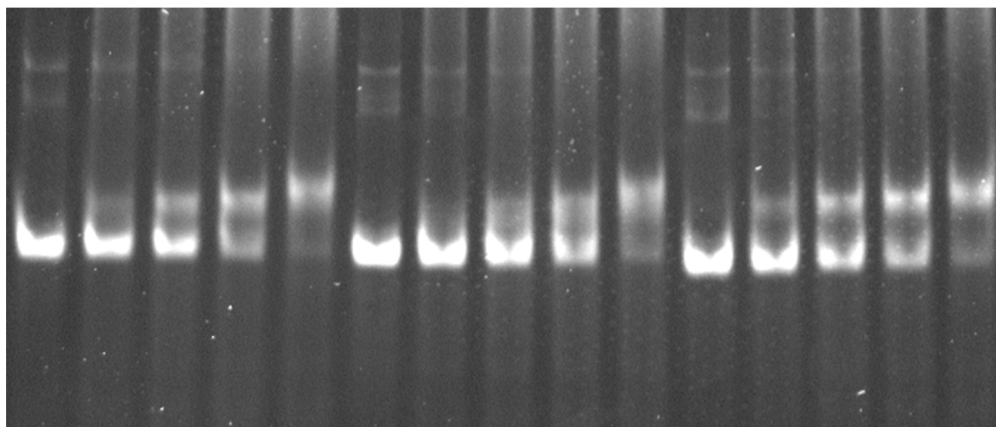
5'-300 nt RNA
NS5Pol

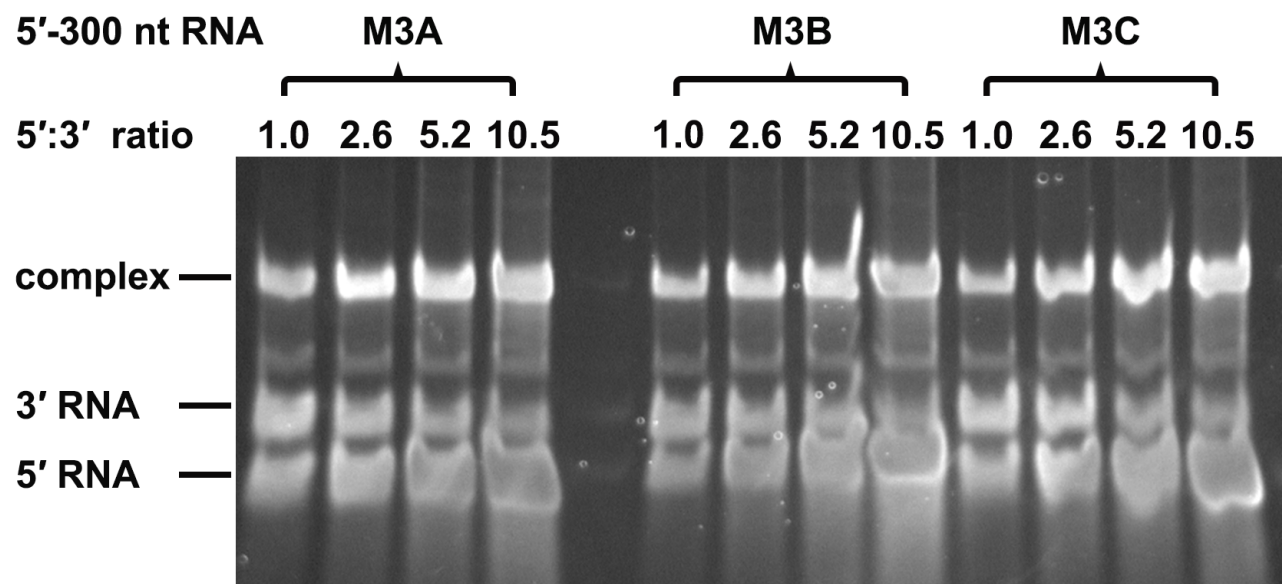
WT

M2A

M2C

complex —
free RNA —



A**B**